

Contents lists available at ScienceDirect

Metabolism

journal homepage: www.journals.elsevier.com/metabolism





Defining lipedema's molecular hallmarks by multi-omics approach for disease prediction in women

Leon G. Straub ^{a,*}, Jan-Bernd Funcke ^a, Nolwenn Joffin ^a, Chanmin Joung ^a, Sara Al-Ghadban ^b, Shangang Zhao ^a, Qingzhang Zhu ^a, Ilja L. Kruglikov ^c, Yi Zhu ^{a,d}, Paul R. Langlais ^{e,f}, Ruth Gordillo ^a, Karen L. Herbst ^{e,g,1,*}, Philipp E. Scherer ^{a,1,2,*}

- ^a Touchstone Diabetes Center, The University of Texas Southwestern Medical Center, Dallas, TX 75390, USA
- ^b Department of Plastic Surgery, Maxillofacial & Oral Health, University of Virginia, Charlottesville, VA 22903, USA
- ^c Scientific Department, Wellcomet GmbH, Bruchsal D-76646, Germany
- ^d Children's Nutrition Research Center, Department of Pediatrics, Baylor College of Medicine, Houston, TX 77030, USA
- ^e The University of Arizona College of Medicine, Division of Endocrinology, Department of Medicine, Tucson, AZ 85724, USA
- f Center for Disparities in Diabetes, Obesity, and Metabolism (CDDOM), University of Arizona Health Sciences, Tucson, AZ 85721, USA
- g The Roxbury Institute, Tucson, AZ 85715, USA

ARTICLE INFO

Keywords: Lipedema Adipose tissue Multi-omics Machine learning Disease prediction Inflammation Complement Random Forest classifier Support vector machine ElasticNet

ABSTRACT

Lipedema is a chronic disease in females characterized by pathologic subcutaneous adipose tissue expansion and hitherto remains without druggable targets. In this observational study, we investigated the molecular hallmarks of lipedema using an unbiased multi-omics approach. We found adipokine dysregulation in lipedema patients participating in a cross-sectional clinical study (ClinicalTrial.gov, NCT02838277), pointing towards the adipocyte as a key player. Analyses of newly generated transcriptomic (SRA, PRJNA940039) and proteomic (ProteomeXchange, PXD058489) datasets of early- and late-stage lipedema samples revealed a local downregulation of factors involved in inflammation. Concomitantly, factors involved in cellular respiration, oxidative phosphorylation, as well as in mitochondrial organization were upregulated. Measuring a cytokine and chemokine panel in the serum of non-menopausal women, we observed little systemic changes in inflammatory markers, but a trend towards increased VEGF. Metabolomic and lipidomic analyses highlighted altered circulating glutamic acid, glutathione, and sphingolipid levels, suggesting a broader dysregulation of metabolic and inflammatory processes. We subsequently benchmarked a set of models to accurately predict lipedema using serum factor measurements (sLPM). Our study of the molecular signature of lipedema thus provides not only potential targets for therapeutic intervention, but also candidate markers of disease development and progression.

1. Introduction

Lipedema is considered a chronic "loose connective tissue" disease [1] that predominantly affects women and manifests in pronounced changes in adipose tissue morphology and consistency in affected areas [2]. Cardinal symptoms include pain, swelling, and easy bruising, typically of the legs and arms [3]. Late-stage lipedema patients experience severe reductions of their mobility and quality of life [1]. In the World Health Organization's 11th revision of the International

Classification of Diseases (ICD-11), lipedema is referred to 'Lipoedema' and assigned the code 'EF02.2'. While prevalent, due to frequent misdiagnosis, the actual incidence rate is estimated to be up to ~ 10 % in women [4,5]. In the 2023 Lipedema Foundation's research roadmap, the "absence of validated and clear druggable targets" led to a call for action [6]. The only widely applied treatment option for lipedema is liposuction [7,8], which remains very effective for plastic reconstruction but can worsen adipose tissue health in the long term [9,10]. The underlying disease causes have remained elusive because lipedema affects a

^{*} Corresponding authors.

E-mail addresses: leon.straub@utsouthwestern.edu (L.G. Straub), drherbst@theroxburyinstitute.com (K.L. Herbst), philipp.scherer@utsouthwestern.edu (P.E. Scherer).

These authors contributed equally to the work.

 $^{^{2}}$ Lead contact.

complex network of different cell and tissue types and presents as distinct stages [4,11]. Disease onset is positively associated with puberty and pregnancy, which suggests a major role of sex hormones like estrogen [12] and cyclical changes in gut wall permeability [13,14]. Heritability has been suggested to be autosomal dominant with sex differences [15]. The progressive appearance of distinct symptoms during lipedema development has led the field to subdivide the disease into 3 stages [1,16]. At stage 1, patients exhibit a normal skin surface but an enlarged hypodermis. At stage 2, the patient's skin becomes uneven and larger mounds of adipose tissue grow as non-encapsulated masses. At stage 3, patients display deformations of the thighs caused by large extrusions of adipose tissue. While lymphedema can occur at any stage of lipedema, it is most frequently observed at stage 3. Allen and Hines proposed that edema formation is a consequence of poor resistance of accumulated adipose tissue against fluid pressure from capillaries into the interstitium [17].

Adipokines regulate a plethora of biological processes, including inflammation and fibrosis, and their secretion is shaped by age, BMI, and menopausal status and could thus play an important role in lipedema manifestation [18]. Adiponectin and leptin are two major adipokines whose levels correlate negatively and positively with BMI, respectively [19]. While adiponectin acts as an insulin-sensitizer and exerts anti-inflammatory and anti-fibrotic functions, leptin acts as a regulator of energy balance and exerts pro-inflammatory and pro-fibrotic functions [20].

In this study, we employed a multi-pronged approach of combined adipose tissue transcriptomics and proteomics as well as serum cytokine and chemokine measurements, metabolomics, and lipidomics to define molecular hallmarks of lipedema. We performed a comprehensive analysis of the gathered data using Metascape [21] to assess *Pattern Gene Database* (PaGenBase) tissue and cell type representation [22], *Gene Ontology* (GO) and *Kyoto Encyclopedia of Genes and Genomes* (KEGG) pathway enrichment [23–26], and *Transcriptional Regulatory Relationships Unraveled by Sentence-Based Text-Mining* (TRRUST) transcription factor enrichment [27]. We furthermore took advantage of these newly acquired, expansive serum factor measurements datasets to train and benchmark multiple lipedema prediction models.

2. Results

2.1. Early lipedema is characterized by disrupted correlations between circulating adipokine levels and BMI

To characterize lipedema development, 72 female lipedema patients (stages 1-3) and 49 female control subjects were compared. As previously published, all individuals consented in writing before enrollment in a study approved by the University of Arizona Human Research and Protection Program [28] (see STROBE diagram in Fig. 1A). The Inclusion Criteria for both groups at enrollment were: sex male or female (only females were analyzed); any race; age of 19-70 years; normal TSH levels; stable body weight in the past 3 months (allowed fluctuation of ±4.5 kg). The Exclusion Criteria at enrollment were: pregnancy; HIV infection; scleroderma, keloid formation, or other skin conditions; cellulitis; bleeding diathesis; use of immunosuppressants or corticosteroids; use of tobacco or marijuana; current weight gain medication (e.g. anti-psychotics); use of NSAIDs, aspirin, histamine (H) 1 blocker, H2 blocker, tetracycline, or corticosteroids within the past 5 days; barium enema within the past 7 days; use of any antibiotic within the past 30 days; blood donation within the past 56 days. A healthy control group was matched for age, sex, race, and BMI. Herein we describe the lipedema study part of the clinical study NCT02838277. As a consequence, individuals with other adipose tissue disorders (e.g. Dercum's disease or familial multiple lipomatosis) were excluded. Subsampling for downstream analyses was required when tissue or serum sample amounts were limited.

Although debatable, in a first approximation, we assumed that

lipedema develops successively from stage 1 to stage 2 and thereafter to stage 3, accompanied by increases in adipose tissue size. We used the following staging criteria: Stage 1, the skin is even and subcutaneous adipose tissue is enlarged with buildups around pelvis, buttocks, hips, and knees; Stage 2, the skin is uneven with indentations in adipose tissue and larger mounds that can be felt (sometimes referred to as lipomas); Stage 3, there are large extrusions of adipose tissue especially at the hips and around the knees. Lipedema patients at stage 1 and control subjects (Table 1) were comparable in their BMI (Fig. 1B), age (Fig. S1A), and menopausal status (Fig. 1C). In contrast, lipedema patients at stages 2 and 3 exhibited a higher BMI and age. While menopausal individuals were, on average, older within all groups (Fig. S1B), differences in BMI between pre-menopausal and menopausal individuals were only observed for lipedema patients at stage 1 (Fig. S1C), which is important regarding adjustments for age in later analyses.

Lipedema development coincides with pronounced changes in adipose tissue anatomy. Serum adipokine concentrations, especially those of adiponectin (ADIPOQ) and leptin (LEP), can provide insights into adipose tissue health. We thus correlated serum ADIPOQ and LEP levels with BMI within each group (Fig. 1D-E). Circulating adiponectin levels have previously been found to correlate negatively with BMI [29,30]. Our control subjects' serum adiponectin levels fell short of being significantly correlated with BMI, but in lipedema patients at stage 1 the correlation was far weaker (Fig. 1D). Compared to control subjects, both p-value and Pearson correlation coefficient (ρ) changed strongly at lipedema stage 1 from 0.09 to 0.62 (p-value) and -0.25 to 0.15 (ρ) (Fig. 1D). The circulating levels of high molecular weight adiponectin (HMW ADIPOQ), a more active form of the hormone, displayed similar trends (Fig. 1F). Overall, the mean ADIPOO levels were comparable between groups, with the exception of lipedema stage 2 (Fig. S1F). Compared to ADIPOQ levels, LEP levels displayed a strong positive correlation with BMI in controls as well as stage 2 and 3 lipedema patients (Fig. 1E, Fig. S1E). However, in stage 1 lipedema patients, a strong disruption of that correlation was observed (Fig. 1E, Fig. S1E).

The lipedema stage 2 and 3 groups contained an increased fraction of menopausal individuals compared to the lipedema stage 1 and control groups (Fig. 1C). Could menopause-associated differences in sex hormones mask part of the effect of lipedema on adipocyte function? To answer that question, we excluded menopausal individuals from our analysis of ADIPOQ and LEP levels. We dropped the stage 3 group altogether, because removing menopausal women represented a too large fraction of that group. Restricting our analyses to pre-menopausal women, the correlations of circulating ADIPOQ levels with BMI became clearer, while those of circulating LEP with BMI remained largely unaffected (Fig. S1D-E). As a consequence of the small sample size, we caution that future studies will be needed to confirm this dissociation of adipokine secretion from adipose tissue mass. However, our data suggests that adipocyte function could be most impacted at the onset of lipedema development, which may be covered up by exacerbated obesity at later stages.

2.2. The lipedema adipose tissue transcriptome exhibits patterns of increased oxidative phosphorylation and decreased leukocyte activation and respiratory burst

We next pursued an unbiased, discovery-driven analysis of the biological processes underlying lipedema development. To this end, we performed RNA sequencing of abdominal and thigh subcutaneous adipose tissue (below a 5 mm punch biopsy) of a BMI- and age-matched subgroup of 14 lipedema patients (stages 1–3) and 7 control subjects without menopause (Fig. 2A, Table S1). We included lipedema patients at stages 1 to 3 because we hypothesized that the biological processes that are central to sustaining the disease are present at all stages. RNA sample or RNAseq data quality was too low for abdominal fat samples of UA0427 and UA0627, and for thigh fat samples of UA0036, UA0624. The total n-number of 21 can be explained by the inclusion 17

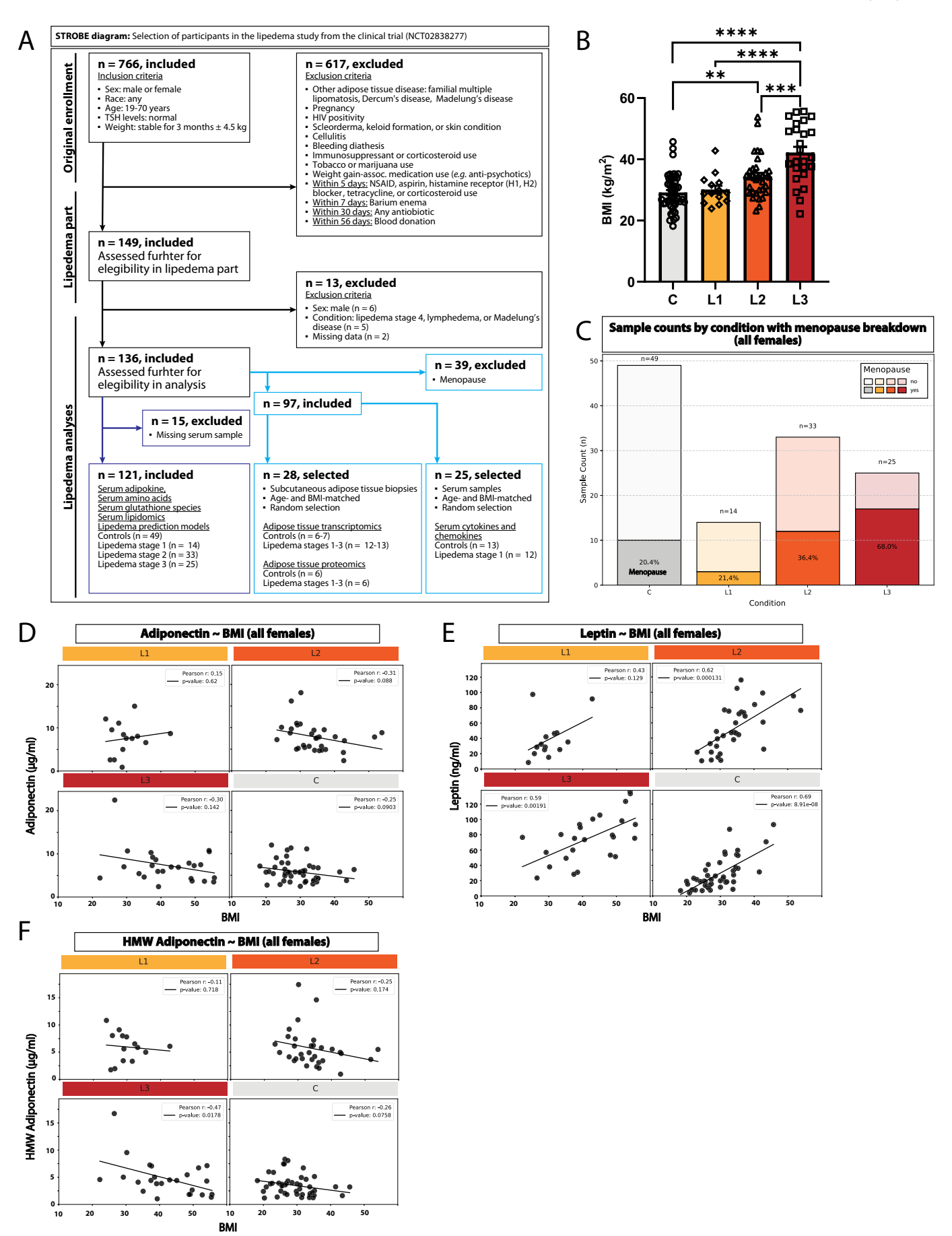


Fig. 1. Early lipedema is characterized by disrupted correlations between circulating adipokine levels and BMI.

(A) STROBE diagram of the clinical study (NCT02838277) with specific focus on the selection of participants in the lipedema study. For serum based analyses (analysis 1), the following groups were analyzed: C, control subjects (n=49); L1, lipedema stage 1 patients (n=14); L2, lipedema stage 2 patients (n=33); L3, lipedema stage 3 patients (n=25). (B) Bar graph of body mass index (BMI). (C) Histogram of study subject count (y-axis = total count) and prevalence of menopause in percent (number inside box). (D-F) Dot plot and correlations of serum adipokines with BMI. Serum adiponectin with BMI (D), serum leptin with BMI (E), and serum high molecular weight (HMW) adiponectin with BMI (F). Data includes all women regardless of menopausal status. Pearson correlation coefficient (rho, ρ) and p-value (p) are given for each subgroup. *Statistics*: (B) Displayed as mean \pm SEM; analyzed by one-way ANOVA (scipy.stats.f_oneway) with correction for multiple testing with FDR Benjamini-Hochberg method (Python: statsmodels.stats.multitest.multipletests method='fdr_bh'). *, FDR < 0.05; ***, FDR < 0.01; ****, FDR < 0.005; *****, FDR < 0.001. (D-F) Pearson correlation (Python: scipy.stats.pearsonr).

Table 1
Characteristics of the groups of participants analyzed in this study.

| Group | n | Sex (M/F) | $\begin{array}{c} {\rm BMI} \\ {\rm (mean\pmSEM)} \end{array}$ | BMI (p-value) | Age (mean \pm SEM) | Age (p-value) | Race (n) |
|-----------------------|----|--------------|--|---|----------------------|---|--|
| Control (C) | 49 | 0/49 | 29.12 ± 0.84 | 'C vs L1', $p = 0.58$ 'C vs L2', $p = 0.0004$ 'C vs L3', $p < 0.00001$ | 38.83 ± 1.92 | 'C vs L1', p = 0.52 'C vs L2', p = 0.0008 'C vs L3', p = 0.00007 | White, 39 Asian, 5 Black, 2 American Indian or Alaska Native/Asian, 2 American Indian or Alaska, 1 |
| Lipedema stage 1 (L1) | 14 | 0/14 | 30.07 ± 1.31 | 'C vs L1', p = 0.58 'L1 vs L2', p = 0.023 'L1 vs L3', p = 0.0002 | 41.21 ± 3.10 | 'C vs L1', $p = 0.52$ 'L1 vs L2', $p = 0.041$ 'L1 vs L3', $p = 0.0084$ | White, 13 Black, 1 |
| Lipedema stage 2 (L2) | 33 | 0/33 | 34.34 ± 1.23 | 'C vs L2', p = 0.0004 'L1 vs L2', p = 0.023 'L2 vs L3', p = 0.0009 | 49.93 ± 2.28 | 'C vs L2', $p = 0.0008$ 'L1 vs L2', $p = 0.041$ 'L2 vs L3', $p = 0.215$ | White, 32 American Indian or Alaskan Native, 1 |
| Lipedema stage 3 (L3) | 25 | 0/25 | 42.15 ± 1.92 | 'C vs L3', $p < 0.00001$ 'L1 vs L3', $p = 0.00017$ 'L2 vs L3', $p = 0.0009$ | 52.76 ± 2.19 | 'C vs L3', p = 0.00007 'L1 vs L3', p = 0.008 'L2 vs L3', p = 0.215 | White, 23 Asian, 1 Black, 1 |

All participants in this study stem from a larger cross-sectional clinical study (NCT02838277).

overlapping patients for thigh and abdominal locations and each two unique IDs for each location. Performing a principal component analysis, we observed no clear clustering of samples based on adipose tissue depot (Fig. 2B). However, a diagonal line could be assumed to divide a more spread cluster of lipedema samples from a less spread of control samples with slight overlap at the edges (Fig. 2B). A separate approach of hierarchical clustering confirmed this trend (Fig. S2A).

The high variation in adipose tissue transcriptome analysis prevented us from finding any differentially expressed genes (DEGs) at the given number of patients when comparing lipedema and control samples at each location separately (Fig. 2C-D). Comparing all samples independent of location, we discovered a total of 296 DEGs (Fig. 2E, Table S2; False Discovery Rate (FDR) < 0.05). Next, we separately queried Metascape with the 144 upregulated, or the 152 downregulated DEGs to analyze our RNAseq data for tissue and cell type representation (PaGenBase), pathway enrichment (GO and KEGG), and transcription factor enrichment (TRRUST).

PaGenBase pattern analysis of this list of DEGs revealed adipose tissue of lipedema patients to be enriched only in expression patterns 'adipose tissue' (Fig. 2F) and depleted of expression patterns including 'blood', 'spleen', 'bone marrow', 'lung', and 'thymus' (Fig. 2G). GO pathway analysis of upregulated DEGs showed an enrichment for 'aerobic respiration', 'cellular respiration', 'oxidative phosphorylation', 'energy derivation by oxidation of organic compounds', 'respiratory electron transport chain', and 'generation of precursor metabolites and energy' (Fig. 2H, Table S3), providing a glimpse into potential causes of lipedema. KEGG pathways found analyzing upregulated DEGs included 'oxidative phosphorylation', 'diabetic cardiomyopathy', 'thermogenesis', 'chemical carcinogenesis - reactive oxygen species', 'Parkinson's disease', 'prion disease', 'Huntington disease', 'Alzheimer's disease', 'non-alcoholic fatty liver disease', 'amyotrophic lateral sclerosis', and 'pathways of neurodegeneration - multiple diseases' (Fig. 2I, Table S3). For downregulated DEGs, GO pathway analysis showed an enrichment for 'leukocyte activation', 'endocytosis', 'cell activation', 'respiratory burst', 'phagocytosis', 'import into cell', 'lymphocyte activation', 'immune effector process', and 'innate immune response' (Fig. 2J, Table S4) and KEGG pathway analysis an enrichment for 'chemokine signaling

pathway', 'Fc gamma R-mediated phagocytosis', 'Leishmaniasis', 'Yersinia infection', 'osteoclast differentiation', 'phagosome', and 'platelet activation' (Fig. 2K, Table S4). Taken together, these pathway analyses suggest a local enhancement of oxidative phosphorylation and cellular respiration as well as suppression of inflammation and immune cell activation in lipedema adipose tissue.

We furthermore investigated enrichment of known transcription factors (TFs) of the DEGs using TRRUST. Only PPARG was found for the upregulated genes (Fig. 2L). For downregulated genes TFs, we found HBP1, SPI1, CEBPA, MYB, SP1, and ETS1 to be enriched (Fig. 2M).

Throughout the literature, the abdominal fat of lipedema patients is often considered to be 'unaffected' while their thigh fat is considered to be 'affected' by the disease. Because there is a great interest in finding differences between the fat residing in these different locations, we used a less rigorous statistical method to define, in a second step, all genes that have a one-way ANOVA p-value smaller than 0.05 as uncorrected differentially expressed genes (uDEGs) (Fig. S2B-G). This constitutes an analysis without correction for multiple testing, thus increasing the number of DEGs but risking a disproportionately high number of false positives. We found similar numbers of uDEGs specific for each location: 814 for abdominal fat, 732 for thigh fat, and 248 overlapping (Fig. S2B). By applying logics to the up- and down-regulated uDEGs that are specific for each location, abdomen or thigh, and the uDEGs that are overlapping for both (Fig. S2C), we attempted to determine to what extend supposedly 'unaffected' differed from 'affected' lipedema adipose tissue. Enrichment refers to how statistically overrepresented a GO term within a set of genes is compared to the expected frequency of that term in the whole genome. A total of 37 GO pathways with a -log(p-value) > 5 were called from uDEGs in both abdominal and thigh fat (also called 'overlapping'), 54 GO pathways were specific for abdominal and not present in thigh fat, and 72 GO pathways were specific for thigh and not present in abdominal fat (Fig. S2D). Adipose tissue from both locations exhibited most significant changes in GO pathways including 'oxidative phosphorylation' and 'cellular respiration' (Fig. S2E). This confirmed previous findings with DEGs of combined depot analysis applying a stricter FDR < 0.05 filter. When removing all the overlapping pathways from analysis, abdominal fat distinctly exhibited changed GO pathways

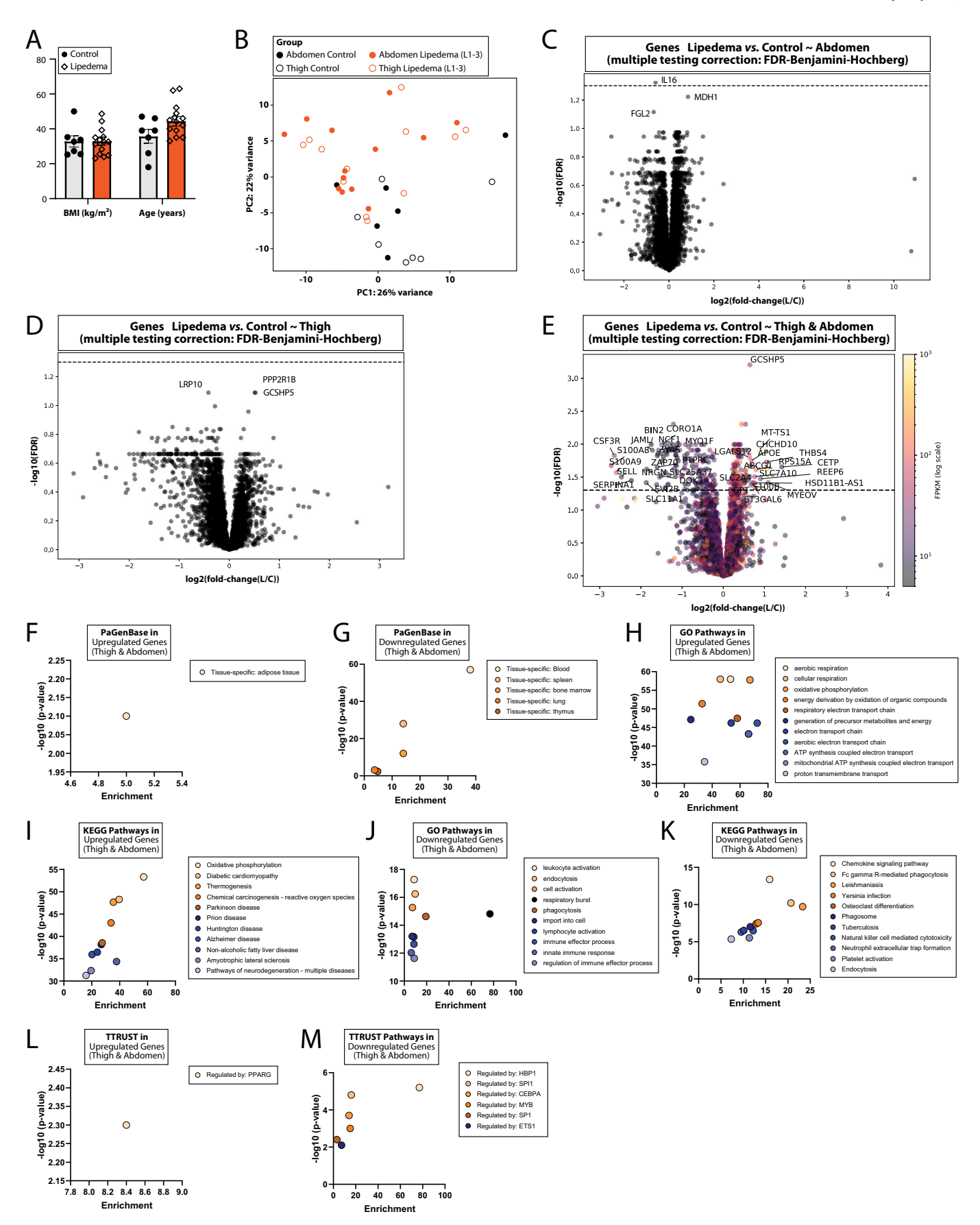


Fig. 2. The lipedema adipose tissue transcriptome exhibits patterns of increased oxidative phosphorylation and decreased leukocyte activation and respiratory burst. The following groups were analyzed: C, control subjects (n = 6 (abdomen)-7 (thigh)); L, lipedema stage 1–3 patients (n = 12 (thigh)-13 (abdomen)). (A) Bar graph of body mass index (BMI) and age. (B) Principal Component Analysis (PCA) of transcriptome data from lipedema and control subcutaneous adipose tissue taken from the abdomen or thigh. (C-E) Volcano plots of differentially expressed genes (DEGs) in abdominal (C), thigh (D), and combined abdominal and thigh (E) adipose tissue depots (FPKM >5). Dotted line indicates FDR < 0.05. (F-G) PaGenBase tissue and cell type representation in upregulated and downregulated DEGs. (J-K) GO and KEGG pathway enrichment in upregulated DEGs. (J-K) GO and KEGG pathway enrichment in downregulated DEGs. (L-M) TRRUST transcription factor enrichment for upregulated and downregulated DEGs. Statistics: (A) Displayed as mean \pm SEM; analyzed by one-way ANOVA (Python: scipy.stats.f_oneway). (B) PCA (Python: sklearn.decomposition.PCA). (C-E) Analyzed by two-sampled t-test (Python: scipy.stats.ttest_ind), multiple comparison correction with FDR Benjamini-Hochberg method (Python: statsmodels.stats.multitest.multipletests method='fdr_bh'). (F-M) Analyzed using Metascape (version 3.5.20240901).

related to 'mitochondrial translation' and 'mitochondrial respirasome assembly' (Fig. S2F), while thigh fat exhibited changed GO pathways related to the 'regulation of actin cytoskeleton organization' (Fig. S2G). To summarize, some transcriptomic changes are unique for each location, but important GO pathways are altered in fat from both locations. This strongly suggests that both adipose tissue depots are affected by lipedema.

2.3. The lipedema adipose tissue proteome validates transcriptomic findings and furthermore suggests local dysfunctions in complement and coagulation cascades

To validate our RNAseq findings, we chose to perform quantitative proteomics comparing global protein expression changes between thigh subcutaneous adipose tissue biopsies (below a 5 mm punch biopsy) from BMI- and age-matched lipedema patients and control subjects (Table S5, Fig. 3A). Only 5 of the respective 28 individuals overlapped between transcriptomic and proteomics analyses (see Table S1 for Patient IDs). Our analysis identified a total of 4987 proteins across 108 fractions from 12 samples. Unbiased Principal Component Analysis (PCA) segregated samples into two distinct groups (Fig. 3B). 171 differentially expressed proteins (DEPs) had an FDR < 0.05 (Table S6). Next, we separately queried Metascape with the 137 upregulated from the 34 downregulated DEPs to analyze our proteomics data for tissue and cell type representation (PaGenBase), pathway enrichment (GO and KEGG), and transcription factor enrichment (TRRUST). The low number of DEPs was not enough for PaGenBase analysis. However, GO pathway analysis of upregulated DEPs demonstrated an enrichment for 'mitochondrial organization', 'mitochondrial membrane organization', 'membrane organization', 'carboxylic acid metabolic process', 'protein localization to organelle', 'intracellular protein transport', and 'cellular respiration' (Fig. 3D, Table S7). Subjecting the list of upregulated DEPs to KEGG pathway analysis revealed an enrichment for 'fatty acid elongation', 'nucleotide metabolism', 'purine metabolism', 'chemical carcinogenesis - reactive oxygen species', 'fatty acid metabolism', 'oxidative phosphorylation' (Fig. 3E, Table S7). Downregulated DEPs were associated with GO pathways including 'humoral immune response mediated by circulating immunoglobulin' and 'complement activation' (Fig. 3F, Table S8) as well as KEGG pathways including 'complement and coagulation cascades', and 'Staphylococcus aureus infection' (Fig. 3G, Table S8). Next, we plotted the -log10(p-value) of the most significant transcriptomic against the respective proteomic GO pathways (Fig. 3H-I). The identified upregulated GO terms 'cellular respiration' and 'oxidative phosphorylation' as well as the downregulated 'immune effector process' and 'leukocyte mediated immunity' feature prominent in both datasets. The low number of DEPs did not allow for a proper TRRUST analysis.

2.4. Lipedema serum measurements indicate mostly unchanged systemic cytokine and chemokine levels, but a trend towards increased VEGFA levels, decreased glutamic acid levels, and increased oxidative stress

To assess whether the suppressed immune cell activation within adipose tissue is reflected or maybe even caused by changes in circulating cytokine and chemokine levels, we utilized a human cytokine and chemokine panel to analyze serum samples of pre-menopausal, BMI- and

age-matched stage 1 lipedema patients (12 individuals) and control subjects (13 individuals) (Table S9). Of the 48 cytokines and chemokines contained in the panel, only three were significantly changed when a less rigorous one-way ANOVA without correction for multiple comparisons was applied (Fig. 4A-B). Specifically, we observed a trend towards reduced IL5 and FLT3L levels, suggesting that B-cell and dendritic cell proliferation and growth and eosinophil activation could be inhibited (Fig. 4A) as well as a trend towards elevated VEGFA levels, suggesting that vascular dysregulation may be present (Fig. 4B). Most importantly, the systemic inflammatory state of lipedema patients appears unchanged.

Next, we measured circulating levels of 31 amino acids for stage 1–3 lipedema patients (72 individuals) and control subjects (49 individuals) (Table 1, Table S1). In an Analysis of Covariance (ANCOVA) with 'age' and 'BMI' as covariates and 'menopausal status' as an independent variable, most amino acid levels were found to be comparable (Fig. 4C-N). Notably though, we observed a significant decrease in glutamic acid across all lipedema stages in comparison to control samples (Fig. 4H). When combining all lipedema stages, methionine sulfoxide was found to be significantly increased (Fig. 4O). Multivariate Analysis of Covariance (MANCOVA) with 'condition' (C, L1, L2 and L3) and 'menopausal status' as independent, categorical variables and 'age' and 'BMI' as continuous covariates revealed that the 'condition' (i.e. lipedema) significantly affects serum amino acid concentrations and that menopause does not cover up these changes (Table 2).

Since glutamic acid is required for the synthesis of glutathione (GSH), an important anti-oxidant factor, we also assessed the circulating levels of reduced and oxidized glutathione (GSSG) using mass spectrometry (Fig. 4P-Q). Reduced glutamic acid levels did not correspond with reduced glutathione serum levels, but a trend towards a reduced GSH/GSSG ratio was apparent (Fig. 4R). MANCOVA with 'condition' (C, L1, L2 and L3) and 'menopausal status' as independent, categorical variables and 'age' and 'BMI' as continuous covariates showed that the 'condition' (i.e. lipedema) and BMI have a significant, but slight effect on serum glutathione concentrations (Table 3).

2.5. Differences in ceramide and sphingolipid metabolism are sufficient to develop accurate serum-based lipedema prediction models

Adiponectin receptors contain a ceramidase domain and their activation has been reported to decrease ceramide and increase sphingolipid levels. Sphingolipids can act as messenger molecules and have been implicated in cardiovascular diseases [31,32]. To gain further insights into lipedema's impact on metabolism, we measured 81 distinct circulating lipids by mass spectrometry, including 10 sphingomyelins, 5 sphingoid bases, 7 lactosyl-ceramides, 7 hexosyl-ceramides, 7 dihydroceramides, 11 ceramides, and 34 sulfatides in serum samples from 72 lipedema patients (stages 1-3) as well as 49 control subjects. Combining lipedema patients of stages 1-3 (Table S10), circulating ADIPOQ and LEP levels were higher compared to control subjects (Fig. 5A-D). We also performed ANCOVA with 'BMI', 'age', or 'BMI & age' as covariates. When adjusting age alone, significance for ADIPOQ was lost, whereas significance for LEP became more pronounced (Fig. 5B). Across all adjustments, serum ceramide species were found to be persistently increased in abundance. As age and menopause are closely related variables, we also performed ANCOVA with 'BMI' as a covariate and

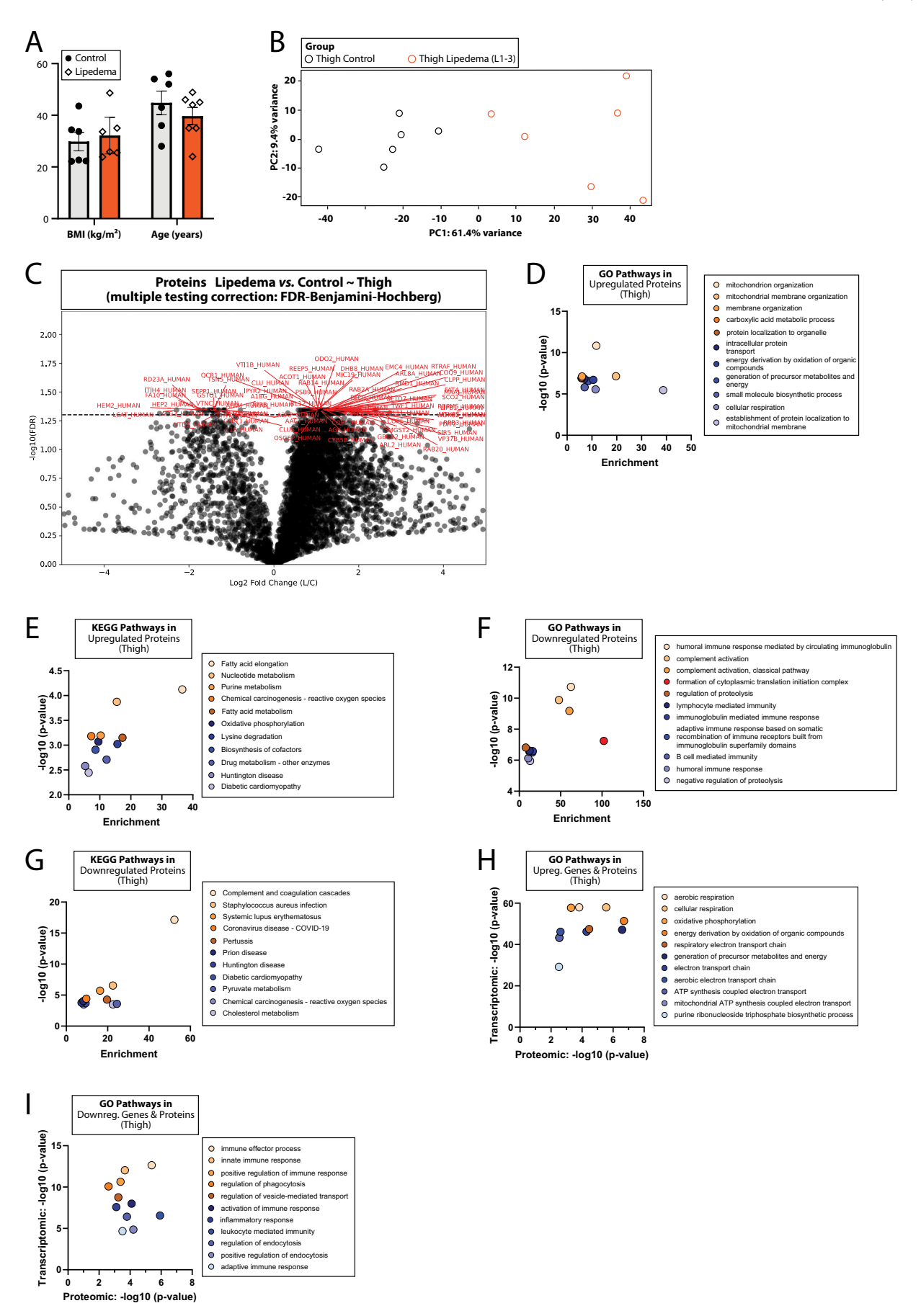


Fig. 3. The lipedema adipose tissue proteome validates transcriptomic findings and furthermore suggests local dysfunctions in complement and coagulation cascades.

The following groups were analyzed: C, control subjects (n = 6); L, lipedema stage 1–3 patients (n = 6). (A) Bar graph of body mass index (BMI) and age. (B) Principal Component Analysis (PCA) of proteome data from lipedema and control subcutaneous adipose tissue taken from the thigh. (C) Volcano plots of differentially expressed proteins (DEPs) in the thigh adipose tissue depot. Dotted line indicates FDR < 0.05. (D-E) GO and KEGG pathway enrichment in upregulated DEPs. (F-G) GO and KEGG pathway enrichment in downregulated DEPs. (H-I) GO pathway enrichment cross-validation between transcriptomic and proteomic results. Analysis of DEGs (combined abdominal and thigh) and DEPs (only thigh). *Statistics*: (A) Displayed as mean \pm SEM; analyzed by one-way ANOVA (Python: scipy.stats.f_oneway). (B) PCA (Python: sklearn.decomposition.PCA). (C) Analyzed by two-sampled t-test (Python: scipy.stats.ttest_ind), multiple comparison correction with FDR Benjamini-Hochberg method (Python: statsmodels.stats.multitest.multipletests method='fdr_bh'). (D-I) Analyzed using Metascape (version 3.5.20240901).

'menopausal status' as an independent variable. This yielded results very similar to those obtained following adjustment for BMI & age (Fig. 5D). This suggests lipedema to have a potential impact on whole body ceramide and sphingolipid metabolism.

MANCOVA with 'condition' (C, L1, L2 and L3) and 'menopausal status' as independent, categorical variables and 'age' and 'BMI' as continuous covariates demonstrated that BMI has the strongest effect on serum ceramide and sphingolipid concentrations (Table 4). We also observed that the effect of the 'condition' (i.e. lipedema) is similar to that of age, with menopause covering up a substantial portion of the effect size as described by Hotelling-Lawley trace and Roy's greatest root statistical tests (Table 4).

The large number of analyzed samples and measured parameters (adipokines and sphingolipids) motivated us to benchmark three different approaches to find an accurate serum lipedema prediction model (sLPM) [33,34]. The following analyses included 121 study participants, irrespective of menopausal status. We used 81 serum lipid parameters as well as 3 adipokines (ADIPOQ, HMW ADIPOQ, and LEP) that we measured (Fig. 5G). We first normalized the data and then divided the samples randomly into training (80 %) and test (20 %) datasets (Python: sklearn.model_selection.train_test_split) [33,34]. The three types of prediction model classifiers were Random Forest Classifier (Python: sklearn.ensemble.RandomForestClassifier), Support Vector Machine (SVM) (Python: sklearn.svm.SVC), and ElasticNet (Python: sklearn.linear_model.ElasticNet) (Fig. 5E).

In the first step, we optimized each individual classifier to model the training dataset as good as possible and in a second step selected the classifier that maximized the F1-score in the test dataset to select a model that shows the lowest false positive rate (FPR) possible. RandomForestClassifier is an ensemble learning method that creates a multitude of decision trees during training but, importantly, corrects for their overfitting to the training dataset. For the test dataset, our F1 scoreoptimized RandomForest model had an F1-score of 76 % (configuration: $n_estimator+10$, random_state = 13, serum parameters scaled with MinMaxScaler (Python: sklearn.preprocessing)) (Fig. S4A). With 89 %, RandomForest had the best recall for control samples, which means that false positive grouping of control subjects as lipedema patients took place in 11 % of the predictions (Fig. 5E). SVM models are supervised max-margin models with associated learning algorithms and known to perform well with noisy data. Our F1-optimized SVM had an F1-score of 80 % (configuration: C = 1, degree = 2, gamma = "auto", kernel="linear", probability = True, random state = 42) (Fig. S4B). With the highest overall accuracy of 80 % (Fig. S4B) and ROC area under the curve of 0.86 (Fig. 5F), our SVM model was better at recalling lipedema patients (81 %), but weaker at recalling controls (78 %) than Random-Forest. ElasticNet is a regularized regression method that linearly combines the penalties of both the lasso and ridge methods. With an overall accuracy of 80 % in the test dataset, a ROC area under the curve of 0.87 (Fig. 5F), and F1-score of 80 %, our F1-optimized ElasticNet correctly recalled 88 % of lipedema patients yet only 67 % of control subjects (Fig. S4C).

One major problem is that we are missing an independent patient cohort, which could function as a validation dataset. A method commonly used to circumvent this problem is called cross-validation (CV), which splits the training dataset into k-folds. To this end, we chose a 5-fold (k=5) cross validation (Python: sklearn.model_selection.

cross_val_score), which means the model was trained using 4 folds and was validated on the last remaining fold. While cross-validation clearly identifies our ElasticNet as an unreliable prediction tool with a CV mean \pm SD value of 0.29 \pm 0.12, our RandomForest and SVM performed much better with respective CV mean \pm SD values of 0.69 \pm 0.11 and 0.78 \pm 0.05 (Fig. 5F).

One can calculate feature importance by permutating the feature columns (different serum parameters) and scoring how much of the predictive power is lost. According to the permutation importance test, RandomForest and SVM both have 31 features with a positive permutation coefficient, while ElasticNet mainly bases its prediction on 6 serum parameters (Fig. 5G). To summarize, key metabolic serum signature could be identified for lipedema patients and two of three models could be benchmarked as good serum-based lipedema prediction tools

3. Discussion

In this study, we provide the first comprehensive, unbiased, multiomics-based systems biology approach to lipedema characterization and diagnosis. By integrating transcriptomic, proteomic, metabolomic, and lipidomic data from a patient cohort of unprecedented size, we define several molecular hallmarks of lipedema and contribute disease prediction models based on serum factor measurements.

A recent family-based study demonstrates genetic heterogeneity in lipedema development, arguing against a single causative exomic factor [35]. In line with this, no reliable genetic test exists for the diagnosis of lipedema. Previous lipedema prediction models were based on the quantification of pain levels [3] or circulating amino acid levels [36]. In the former case [3], it must be acknowledged that pain levels are subjective and can be influenced by unrelated physiological and psychological processes. In the latter case [36], the utilized control groups may not have been properly matched, exacerbating the apparent predictive power of the model. We present 3 distinct serum factor measurementbased lipedema prediction models (sLPM) with good accuracies. We trained our models on all lipedema stages and irrespective of menopausal status to create the most widely applicable prediction tool. Placing the performance of our sLPM into perspective, serum measurement-based or clinical parameter-based prediction models have been tested across multiple diseases other than lipedema with similar F1-scores, control group recall values, and accuracies [37]. Further improvements and validation of the models using independent patient cohorts of multiple study centers would be important before it could be used in the clinics. However, the inaccuracies of the prediction tool could also be caused by lipedema being a disease category that combines distinct disease subgroups that differ at the molecular level.

Even on basic disease parameters, a consensus remains to be found for lipedema. Some investigators have reported adipocyte hypertrophy to be a hallmark of the disease [38], whereas others claim adipocyte hyperplasia to be more prevalent [39]. Adipocyte diameter appears to have a direct impact on adipokine secretion and is an important parameter when judging the healthiness of adipose tissue [40,41]. Adiponectin secretion increases with adipocyte hyperplasia, while adipocyte hypertrophy decreases adiponectin secretion and increases leptin secretion in turn [42]. Previous reports of elevated circulating adiponectin levels in lipedema may be explained by group differences in

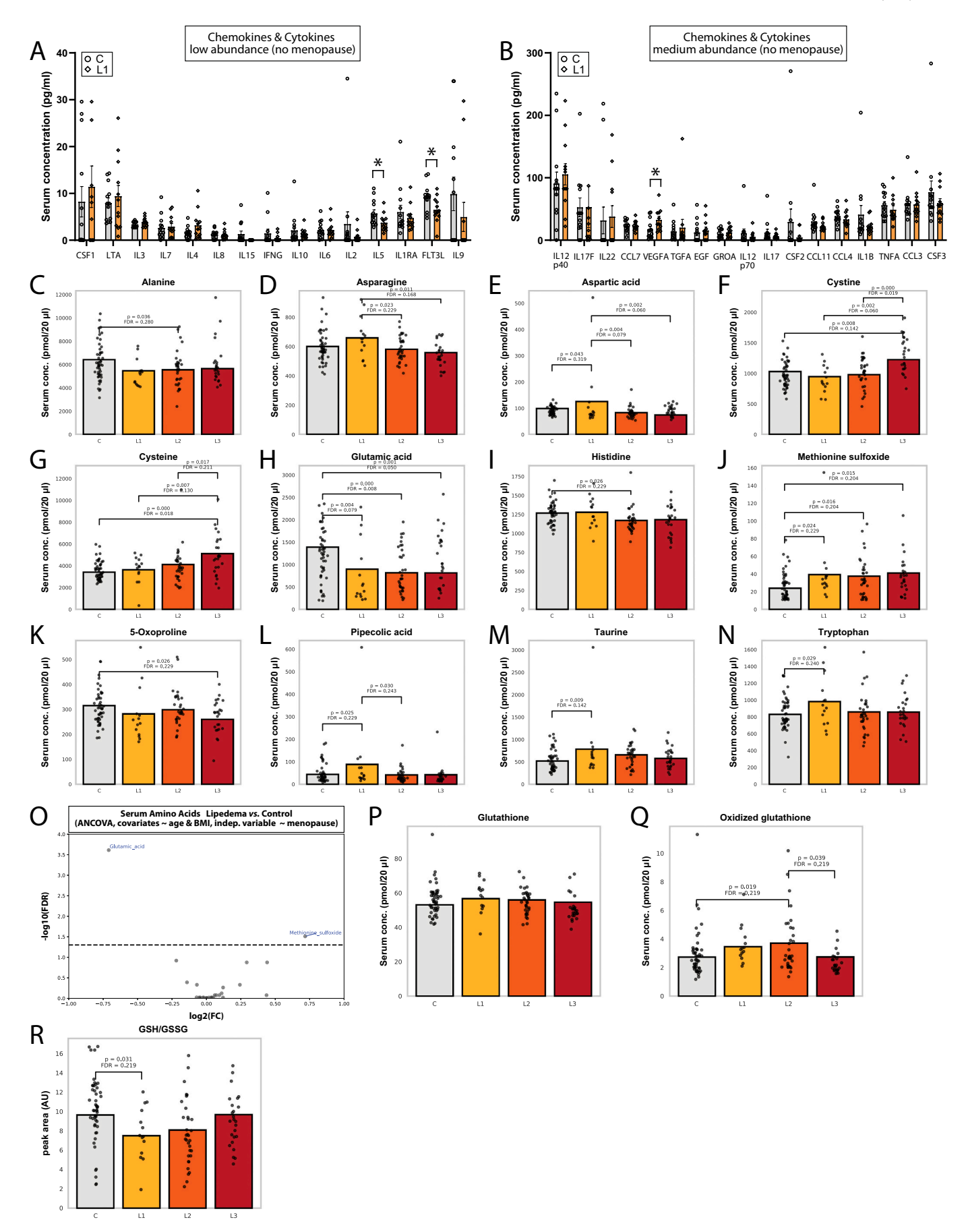


Fig. 4. Lipedema serum measurements indicate mostly unchanged systemic cytokine and chemokine levels, but a trend towards increased VEGFA, decreased glutamic acid, and increased methionine sulfoxide levels.

(A-B) Bar graphs of serum cytokines and chemokines in lipedema stage 1 patients (L1, n=12) and control subjects (C, n=13), menopausal women were excluded. Factors were grouped by abundance: low abundance (A), medium abundance (B). (C-R) ANCOVA of serum amino acids and glutathione species with 'age' and 'BMI' as covariates and 'menopausal status' as an independent variable in control subjects (C, n=49), lipedema stage 1 patients (L1, n=14), lipedema stage 2 patients (L2, n=33), and lipedema stage 3 patients (L3, n=25). (C-N) Bar graphs of serum amino acids. (O) Volcano plot of serum amino acids. Dotted line indicates FDR < 0.05. (P-R) Bar graphs of serum glutathione species and glutathione (GSH)/oxidized glutathione (GS-SG) ratio. *Statistics*: (A-B) Displayed as mean \pm SEM; analyzed by one-way ANOVA. *, p < 0.05. (C-R) Displayed as mean (bar graphs); analyzed by ANCOVA (Python: statsmodels.formula.api.smf.OLS), multiple comparison correction with FDR Benjamini-Hochberg method (Python: statsmodels.stats.multitest.multipletests method='fdr_bh'). p-values and FDRs are given as label where either is significant.

Table 2Multivariate Analysis of Covariance (MANCOVA) of serum amino acids with 'age' and 'BMI' as continuous covariates and 'condition' (C, L1, L2, L3) and 'menopausal status' as independent, categorical variables (related to Fig. 4).

Value Num DF Den DF F Value Pr > FIntercept Wilks' lambda 0.1331 31 83 17.437 0.0000 0.8669 31 83 17.437 0.0000 Pillai's trace. Hotelling-Lawley trace 6.5126 31 83 17,437 0.0000 Roy's greatest root 6.5126 31 17.437 0.0000 83 C (condition) 0.6010 31 83 0.0205 Wilks' lambda 1.7776 Pillai's trace 0.3990 31 83 1.7776 0.0205 Hotelling-Lawley trace 0.6639 1.7776 0.0205 31 83 0.6639 83 1.7776 0.0205 Roy's greatest root C (menopausal status) Wilks' lambda 0.7524 31 83 0.8809 0.6459 Pillai's trace 0.2476 31 83 0.8809 0.6459 Hotelling-Lawley trace 0.3290 31 0.8809 0.6459 83 0.8809 0.3290 31 0.6459 Roy's greatest root 83 BMI Wilks' lambda 3.7988 0.0000 0.4134 31 83 0.5866 31 3.7988 0.0000 Pillai's trace 83 Hotelling-Lawley trace 3.7988 1.4188 31 83 0.0000 Roy's greatest root 1.4188 31 3.7988 0.0000 83 Age Wilks' lambda 83 0.0302 0.6121 31 1.6967 Pillai's trace 0.3879 31 83 1.6967 0.0302 Hotelling-Lawley trace 0.6337 1.6967 0.0302 31 83 Roy's greatest root 0.6337 83 1.6967 0.0302

average adipocyte size and/or overall adipose tissue mass [43]. Appropriate matching of the study cohort is vital for meaningful analyses. In general, we matched our study subjects by multiple parameters. The disruption of adipocyte function in lipedema was most apparent when correlating adiponectin and leptin levels with BMI separately for each lipedema stage and when taking the menopausal status into account. In addition, we found that menopause covers up parts of lipedema-associated changes in serum ceramide and sphingolipid species. This hints at estrogen potentially playing a role in shaping the lipedema phenotype in the local adipose tissue environment, as well as on the systemic ceramide metabolism level. This is one of the first molecular findings to support the long-hypothesized role of sex hormones in lipedema development [12].

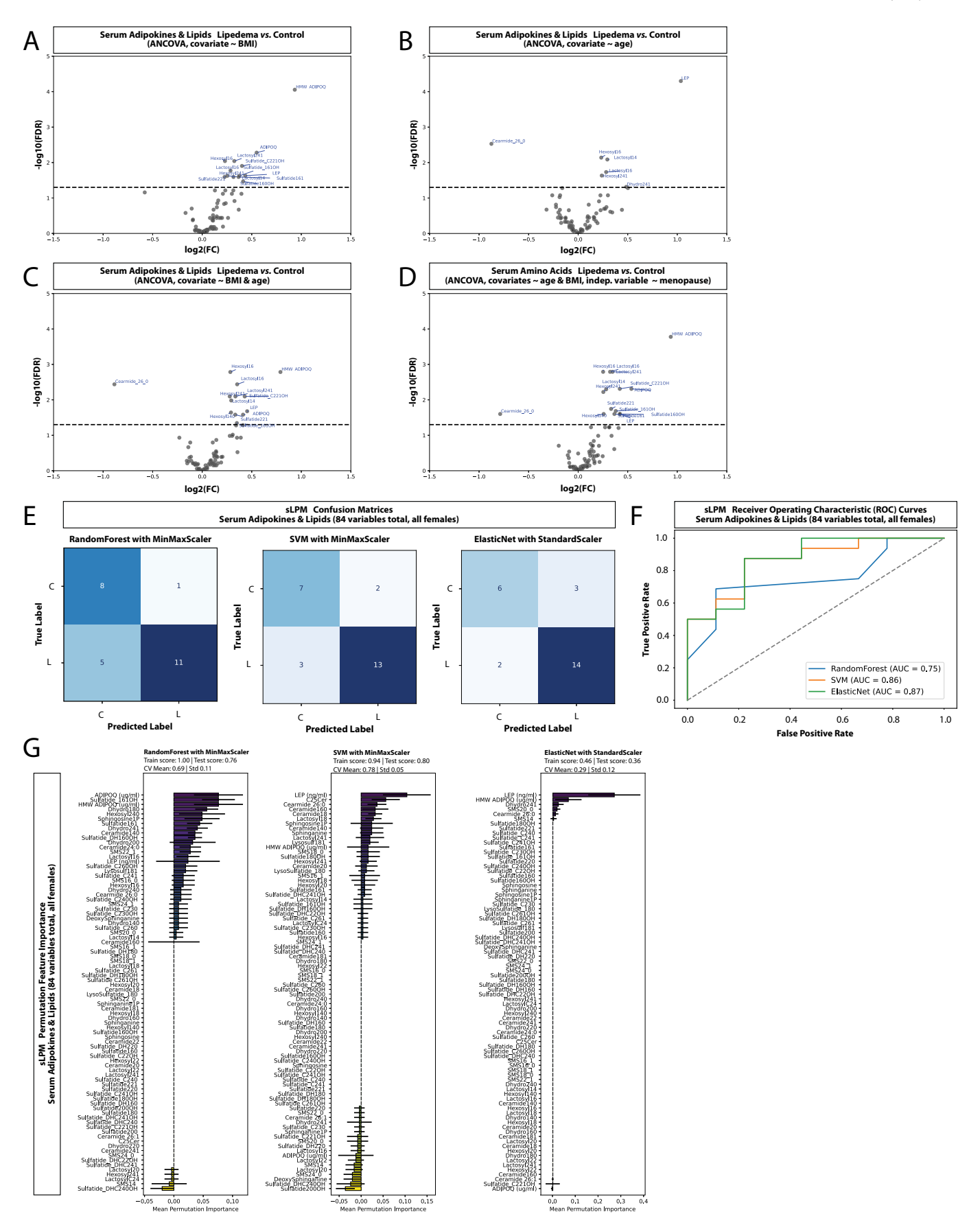
Our observations of disrupted adipokine secretion indicate that adipose tissue function is affected from early on in lipedema development at stage 1. Analyzed across all stages, lipedema patients displayed increased adiponectin in serum, which coincided with distinct changes in different lipid species, including lactosyl- and hexosyl-ceramides. The elevated levels of these specific lipid species could be a consequence of either increased glucosylceramide synthase or decreased glucosylceramidase activity. Adiponectin receptors (ADIPORs) display ceramidase activity [44,45]. Thus, higher adiponectin levels should result in overall

Table 3Multivariate Analysis of Covariance (MANCOVA) of serum glutathione species with 'age' and 'BMI' as continuous covariates and 'condition' (C, L1, L2, L3) and 'menopausal status' as independent, categorical variables (related to Fig. 4).

| | Value | Num DF | Den DF | F Value | Pr > I |
|------------------------|---------|--------|--------|----------|--------|
| Intercept | | | | | |
| Wilks' lambda | 0.0400 | 5 | 109 | 523.8208 | 0.000 |
| Pillai's trace | 0.9600 | 5 | 109 | 523.8208 | 0.000 |
| Hotelling-Lawley trace | 24.0285 | 5 | 109 | 523.8208 | 0.000 |
| Roy's greatest root | 24.0285 | 5 | 109 | 523.8208 | 0.000 |
| C (condition) | | | | | |
| Wilks' lambda | 0.8185 | 5 | 109 | 4.8333 | 0.000 |
| Pillai's trace | 0.8183 | 5 | 109 | 4.8333 | 0.000 |
| Hotelling-Lawley trace | 0.1813 | 5 | 109 | 4.8333 | 0.000 |
| Roy's greatest root | 0.2217 | 5 | 109 | 4.8333 | 0.000 |
| Roy's greatest 100t | 0.2217 | 3 | 109 | 4.6555 | 0.000 |
| C (menopausal status) | | | | | |
| Wilks' lambda | 0.9217 | 5 | 109 | 1.8525 | 0.108 |
| Pillai's trace | 0.0783 | 5 | 109 | 1.8525 | 0.108 |
| Hotelling-Lawley trace | 0.0850 | 5 | 109 | 1.8525 | 0.108 |
| Roy's greatest root | 0.0850 | 5 | 109 | 1.8525 | 0.108 |
| BMI | | | | | |
| Wilks' lambda | 0.9012 | 5 | 109 | 2.3895 | 0.042 |
| Pillai's trace | 0.0988 | 5 | 109 | 2.3895 | 0.042 |
| Hotelling-Lawley trace | 0.1096 | 5 | 109 | 2.3895 | 0.042 |
| Roy's greatest root | 0.1096 | 5 | 109 | 2.3895 | 0.042 |
| Age | | | | | |
| Milks' lambda | 0.9283 | 5 | 109 | 1.6836 | 0.144 |
| Pillai's trace | 0.0717 | 5 | 109 | 1.6836 | 0.144 |
| Hotelling-Lawley trace | 0.0717 | 5 | 109 | 1.6836 | 0.144 |
| Roy's greatest root | 0.0772 | 5 | 109 | 1.6836 | 0.144 |
| noy a greatest root | 0.0772 | 3 | 109 | 1.0030 | 0.14 |

lower ceramide levels, which was not the case in our lipedema patients. Either lipedema is accompanied by adiponectin resistance, or ceramides are generated faster than they can be degraded, hence a compensatory upregulation of the adiponectin/AdipoR axis as a compensatory mechanism.

Elevated serum ceramide levels are widely considered to be associated with negative health outcomes [31,46]. Ceramide C22:0, C20:0, and C18:0 correlate negatively with adiponectin levels and positively with HOMA-IR, BMI z-score, as well as triglyceride and fasting blood glucose levels [47]. In addition, a negative correlation between ceramide C16:0 and circulating adiponectin was reported [48]. Ceramides and sphingoid bases are important metabolic messengers that also contribute to regulation of apoptosis, oxidative stress, and the immune response [49,50], as highlighted by the use of the sphingosine analogue fingolimod for multiple sclerosis treatment [51]. Glycosylceramides are suggested to activate immune cell function, for example through LPS/ TLR4 complex orientation [52,53]. Related to LPS/TLR4 signaling, we recently proposed the accumulation of bacterial LPS in gluteofemoral adipose tissue to be a driving force of lipedema development [54]. While we could not measure these parameters in our lipedema serum samples, our findings related to changes in complement and coagulation pathways are in agreement with this hypothesis.



(caption on next page)

Fig. 5. Lipedema serum measurements indicate changes in ceramide and sphingolipid metabolism and serum lipid measurements can be used to build accurate lipedema prediction models.

The following groups were analyzed: C, control subjects (n = 49); L, lipedema stage 1–3 patients (n = 72). (A-D) ANCOVA of serum lipids and adipokines with 'BMI' as a covariate (A), 'age' as a covariate (B), 'BMI' and 'age' as covariates (C), or 'BMI' as a covariate and 'menopausal status' as an independent variable (D). Volcano plots are provided. Dotted lines indicate FDR < 0.05. (E-G) Benchmarking of three distinct supervised learning methods: RandomForest, Support Vector Machine (SVM), and ElasticNet. Confusion Matrices (E) and Receiver Operating Characteristic (ROC) curves (F) of the different serum factor measurement-based lipedema prediction models (sLPM) are given. Analyzed data was adjusted for age. (G) Permutation Feature Importance depicted as vertical bar graphs. *Statistics*: (A-D) Analyzed by ANCOVA (Python: statsmodels.formula.api.smf.OLS), multiple comparison correction with FDR Benjamini-Hochberg method (Python: statsmodels.stats. multitest.multipletests method='fdr_bh'). (E) Confusion Matrices (Python: sklearn.metrics.confusion_matrix). (F) Receiver Operating Characteristic curves (Python: sklearn.metrics.roc_curve). (G) Cross-Validation (Python: sklearn.model_selection cross_val_score) and Permutation Feature Importance (Python: sklearn.inspection. permutation_importance). Displayed as mean \pm SD.

Table 4Multivariate Analysis of Covariance (MANCOVA) of serum lipids with 'age' and 'BMI' as continuous covariates and 'condition' (C, L1, L2, L3) and 'menopausal status' as independent, categorical variables (related to Fig. 4).

| | Value | Num DF | Den DF | F Value | Pr > F |
|------------------------|---------|--------|--------|---------|--------|
| Intercept | | | | | |
| Wilks' lambda | 0.0291 | 49 | 68 | 46.2259 | 0.0000 |
| Pillai's trace | 0.9709 | 49 | 68 | 46.2259 | 0.0000 |
| Hotelling-Lawley trace | 33.3099 | 49 | 68 | 46.2259 | 0.0000 |
| Roy's greatest root | 33.3099 | 49 | 68 | 46.2259 | 0.0000 |
| | | | | | |
| C (condition) | | | | | |
| Wilks' lambda | 0.1666 | 50 | 67 | 6.7046 | 0.0000 |
| Pillai's trace | 0.8334 | 50 | 67 | 6.7046 | 0.0000 |
| Hotelling-Lawley trace | 5.0034 | 50 | 67 | 6.7046 | 0.0000 |
| Roy's greatest root | 5.0034 | 50 | 67 | 6.7046 | 0.0000 |
| | | | | | |
| C (menopausal status) | | | | | |
| Wilks' lambda | 0.2472 | 50 | 67 | 4.0814 | 0.0000 |
| Pillai's trace | 0.7528 | 50 | 67 | 4.0814 | 0.0000 |
| Hotelling-Lawley trace | 3.0458 | 50 | 67 | 4.0814 | 0.0000 |
| Roy's greatest root | 3.0458 | 50 | 67 | 4.0814 | 0.0000 |
| | | | | | |
| BMI | | | | | |
| Wilks' lambda | 0.0986 | 50 | 67 | 12.2479 | 0.0000 |
| Pillai's trace | 0.9014 | 50 | 67 | 12.2479 | 0.0000 |
| Hotelling-Lawley trace | 9.1402 | 50 | 67 | 12.2479 | 0.0000 |
| Roy's greatest root | 9.1402 | 50 | 67 | 12.2479 | 0.0000 |
| | | | | | |
| Age | | | | | |
| Wilks' lambda | 0.1775 | 50 | 67 | 6.2074 | 0.0000 |
| Pillai's trace | 0.8225 | 50 | 67 | 6.2074 | 0.0000 |
| Hotelling-Lawley trace | 4.6324 | 50 | 67 | 6.2074 | 0.0000 |
| Roy's greatest root | 4.6324 | 50 | 67 | 6.2074 | 0.0000 |

Adipocyte hypertrophy is commonly associated with an infiltration of immune cells and the establishment of a pro-inflammatory environment in adipose tissue [55]. Clinicians report that the adipose tissue of lipedema patients feels softer than that of control subjects [1]. Changes in extracellular matrix (ECM) composition and organization contribute to stiffening of a fibrotic tissue, which often is the result of cyclic inflammation. Fibrosis can be understood as a pathologic form of wound healing that leads to excessive ECM deposition and tissue scarring [56]. Lipedema disease gene pathways and their protein components are still unknown. Only a few reports on the diseased adipose tissue transcriptome have been published [39,57,58]. To our knowledge, this is the first study to indicate that lipedema coincides most strongly with increased gene and protein signatures of cell respiration, mitochondrial function, and oxidative phosphorylation as well as decreased signatures of immune effector processes and complement and coagulation cascades. In contrast to our findings, several previous reports suggested that increased inflammation would be a hallmark of lipedema adipose tissue [57–62]. Based on our data, we now hypothesize that the exclusion of immune cells from subcutaneous lipedema adipose tissue or the suppression of their activity is a key hallmark of the disease. Signs of reduced complement activation and diminished coagulation could be

interpreted as further evidence supporting the notion of a local suppression of the immune response [63,64]. In fact, we recently proposed that an endotoxin-complement cascade may play an integral role in the regulation of adipocyte cellularity and that reduced complement activity may be at the very source of the adipose tissue expansion in lipedema patients [65]. That the complement and coagulation pathways show up in the top 11 most affected proteomic but not transcriptomic pathways is to be expected, because the process of coagulation is primarily regulated on the protein level [54,66]. During the progression from early stages of lipedema to a more chronic manifestation of the disease pronounced adipose tissue damage accumulates. At stage 3 and in individuals that develop excessive fibrosis, damage to the adipose tissue may advance lymphedema development [28]. Importantly, lymphedema certainly induces immune cell infiltration [67]. We thus suggest that immune cell infiltration may occur as a consequence of co-occurring lymphedema, while our transcriptomic data questions its causative role in lipedema development and maintenance.

Adipose tissue pressure pain is a prevalent observation in lipedema patients [3]. Although pain levels were not assessed in this study, gene and protein signatures were found in lipedema patients that are connected to neurodegeneration. Future clinical lipedema studies should combine pain level measurements with multi-omics approaches.

Our measurements of circulating amino acid levels in lipedema patients led to another key finding, reduced glutamic acid levels. Previous reports on changes in pyruvic acid, phenylalanine, and histidine levels were however not confirmed [36]. The observed changes in glutamic acid levels and associated metabolic processes may constitute a link between metabolic dysfunction and reduced inflammation in lipedema adipose tissue. In tendon injury models, glutamate was found to regulate mast cell function [68]. Glutamic acid is crucial for basic immune cell functions, including lymphocyte proliferation and cytokine production, macrophage phagocytic and secretory activities, and neutrophil bacterial killing [69]. As such, clinical nutritional protocols for pre- and postoperative treatment unrelated to lipedema include glutamic acid supplementation [70,71]. The glutamine dipeptides L-alanyl-1-glutamine (Ala-Gln), cleaved by human plasma amino peptidases, is the most suitable precursor of glutamic acid for nutritional supplementation [71]. Future clinical research with glutamine dipeptide supplementation of lipedema patients could investigate this potential link between metabolic and immune functions, potential in combination with liposuction surgery. There is indeed a pressing need for studying the response of individual lipedema symptoms to more common forms of therapy [12]. Immune-modulating drug and anti-histamine trials in women with lipedema, as identified as a priority by the Lipedema Foundation, are not supported by our finding that adipose tissue inflammation is actually reduced in lipedema patients compared to properly-matched control subjects.

To conclude, our multi-omics approach allows us to present comprehensive molecular disease hallmarks. The high resolution of our analysis allowed us to not only hypothesize gene ontology pathways, but also discover genes and proteins previously unrelated to lipedema disease ontology and manifestation. Focusing on these molecular links could be instrumental to develop new lipedema treatment strategies.

3.1. Limitations of the study

Because this study is cross-sectional, we cannot draw firm conclusions regarding the contribution of specific factors and processes we identified to lipedema development and maintenance. For the analysis of disease pathway overlap, we chose to include patients from all lipedema stages in these analyses to discover candidate mechanisms that sustain lipedema, potentially biasing against mechanisms involved in early-stage lipedema development. Due to study-inherent challenges in collecting sufficient adipose tissue samples from all participants, our proteomic and transcriptomic analyses were performed not in one and the same subgroup, but in two overlapping subgroups that were sampled from the larger study cohort. In detail, only 5 of the respective 12 individuals analyzed by proteomics were overlapping. This could have increased data variability, especially when comparing proteomic and transcriptomic changes. We are sharing our proteomic and transcriptomic primary data hoping that doing so will allow other researchers to add our data to their own analyses. To reach higher levels of accuracy and further test our new lipedema prediction models, additional multi-center patient samples and data will need to be integrated. In addition, we caution that additional validation datasets are important to estimate the clinical robustness of the lipedema prediction tools that we provide.

4. Methods

4.1. Participants

All women gave written informed consent before enrolling in a study approved by the University of Arizona Human Research and Protection Program [28]. This manuscript describes the lipedema portion of that cross-sectional clinical study (NCT02838277), which took place between June 2016 and October 2019. Further details can be found at cl inicaltrial.gov (https://clinicaltrials.gov/ct2/show/NCT02838277). The Human Subjects Protection Program (HSPP), as the administrative and regulatory support program to the Institutional Review Boards (IRBs), works in collaboration with the research community to maintain an ethical and compliant research program. An IRB reviewed all research and related activities involving human subjects conducted during this study. The University of Arizona HSPP has been accredited by the Association for Accreditation of Human Research Protection Programs (AAHRPP) since 2005. No harm was inflicted on the participants as part of the study.

4.1.1. Inclusion criteria

Ambulatory males and/or females able to understand the consent process; of any race; 19–70 years of age; diagnosis of lipedema; individuals without a fat disorder (will be matched by age, sex, race, and body mass index); weight stable for past 3 months within a 10 pound range per personal report of the subject; overweight or obese with BMI $>\!26\,{\rm kg/m^2}$ in order to be able to get enough subcutaneous adipose tissue for the biopsy; individuals with BMI $<\!26\,{\rm kg/m^2}$ may participate in all aspects of the study protocol except the subcutaneous adipose tissue biopsy; thyroid levels in the normal range as confirmed by a TSH measurement; may have treated hypothyroidism that is stable over 6 months.

4.1.2. Exclusion criteria

HIV infection (because of the associated lipodystrophy and fatty growths [lipomas]); subjects will be excluded from having a subcutaneous adipose tissue biopsy with any history of scleroderma, keloid formation, or other skin condition that would result in substantial scarring after biopsy; a history of recurrent cellulitis; other adipose tissue diseases (e.g. Dercum's disease, Familial Multiple Lipomatosis, or Madelung's disease); any history of bleeding diathesis that would place the subject at great risk for persistent bleeding after a biopsy/

liposuction; any history of major complication after a previous biopsy including requirement of a blood transfusion, hospitalization, failure to heal, or major infection requiring intravenous antibiotics, or anyone whose skin and tissue would put them at risk for an infection after the biopsy per the assessment of study staff and the principal investigator; these individuals may participate in the remainder of the protocol, just not the subcutaneous adipose tissue biopsy; use of any immunosuppressant or corticosteroid medication; use of any anti-inflammatory medication such as NSAIDs, aspirin, histamine (H) 1 blocker, H2 blocker, tetracycline, or corticosteroids within five days of the study procedure visit; use of medications that might cause weight gain (e.g. second generation anti-psychotics); blood donation <56 days prior to screening visit; tobacco or marijuana use which may alter inflammation in the body; any antibiotics within the last month, barium enema in the last week which would affect gut bacteria and the MRI; pregnancy due to the risks associated with the fat biopsy in the area of the fetus and because pregnancy will alter hormone levels; women without lipedema were matched by age and body mass index (BMI) to women with lipedema as a comparison group.

Initial matching during recruitment phase was done using MedCalc Statistical Software (MedCalc Software Ltd., Ostend, Belgium). Adjustments for BMI and/or age were implemented by multivariate regression analysis (ANCOVA or MANCOVA). Women were considered to be obese if their BMI was $\geq 30 \,\mathrm{kg/m^2}$. Participant's information on sex (assigned at birth), age, and race was self-reported. Information on gender and socioeconomic status was not collected. For reasons of statistical stringency only women with lipedema stages 1 to 3 and female control subjects were considered for the analyses. Heterogeneity in race was allowed for all groups, but mostly white women participated in the study. The number of subjects does not allow for subgrouping for differences in race. Two participants were excluded for missing key anthropometrics data. Additionally, subgrouping was done according to the menopausal status of women. Throughout the clinical study, we abided by the principles of WMA's Declaration of Helsinki as revised in 2013.

4.2. Biopsies

From January 2017 to October 2019, clean subcutaneous adipose tissue samples without skin were taken from underneath a 5 mm punch biopsies at the thigh and/or abdomen of women with and without lipedema. Serum was collected as well.

4.3. RNA sequencing analysis

RNA was isolated from human adipose tissue with TRIzol reagent (Invitrogen, #15596026) according to the manufacturer's instructions. Total RNA was submitted to Novogene, where quality control and library preparation as well as sequencing was done as described in brief in the following. RNA libraries were build following poly(A) capture and reverse transcription to create cDNA fragments of 150 bp. According to Novogene, paired-end sequencing was performed on a Illumina Novo-Seq platform. RNA sequencing primary data was deposited at htt ps://www.ncbi.nlm.nih.gov/sra with the dataset PRJNA940039. RNA sequencing results stored in the Fastq files were analyzed using the BICF RNASeq Analysis Workflow (Version publish_0.5.15 - https://git.biohpc.swmed.edu/BICF/Astrocyte/rnaseq) of the UT Southwestern Astrocyte Workflow System. In short, this pipeline: (1) trims the ends of sequences with remaining adapter or quality scores <25 and removes any sequence <35 bp after trimming, (2) aligns trimmed Fastq files to the human reference genome (GRCh38) using HiSAT2, 3) Marks duplicates using SAMBAMBA, 4) counts features (genes, transcripts, and exons) using FeatureCounts and StringTie using the Gencode feature table, 5) performs basic pairwise differential expression analysis using EdgeR and DESeq, and 6) calculates abundances of transcripts using ballgown. Significantly regulated genes were

assessed by Bonferroni multiple comparison corrected p-value<0.05. Metascape [21] was used to perform tissue and cell type representation (PaGenBase), pathway enrichment (GO and KEGG), and transcription factor enrichment (TRRUST) analyses.

4.4. Metabolomics (sphingolipids, free amino acids, and sulfatides)

Mass spectrometry-based analyses were performed at the UT Southwestern Metabolic Phenotyping Core mass spectrometry facility.

4.4.1. Sphingolipids were extracted from serum samples as follows

50 µl of serum were added to 4.0 ml organic extraction solvent (isopropanol:ethyl acetate, 15:85; v:v). Immediately afterward, 20 μ l internal standard solution was added (Ceramide/Sphingoid Internal Standard Mixture II at a 10 fold dilution in methanol combined with a mixture of C16 ceramide-d7 (d18:1-d7/16:0), C18 ceramide-d7 (d18:1d7/18:0), C24 ceramide-d7 (d18:1-d7/24:0), and C24:1 ceramide-d7 (d18:1-d7/24:1(15Z)) at a concentration of 2.4 μM ; Avanti Polar Lipids, Alabaster, AL). The mixture was vortexed and 3.0 ml of HPLC water was added. Two-phase liquid extraction was performed, the supernatant was transferred to a new tube, and the aqueous phase was reextracted. Supernatants were combined and evaporated under nitrogen. The dried residue was reconstituted in 200 µl of MeOH. Sphingolipid profiling was conducted by liquid chromatography-electrospray ionization-tandem mass spectrometry (LC-MS/MS), using a Nexera X2 UHPLC coupled to an LCMS-8060 (Shimadzu Scientific Instruments, Columbia, MD, USA). 3 µl and 1 µl of sample was injected for the analysis of sphingoid bases and ceramides, and sphingomyelins, respectively and the autosampler was kept at 9 °C during the duration of the batch analysis. Lipid separation was achieved by reverse-phase liquid chromatography on a 2.1 \times 150 mm, 2.7 μm Ascentis Express C8 HPLC column (Supelco, Bellefonte, PA) using a gradient elution with H_2O 5 mM ammonium formate 0.8 % formic acid (ν/ν) and MeOH 5 mM ammonium formate 0.8 % formic acid (v/v).

4.4.2. Free amino acids were extracted from serum as follows

15 μ l of serum was added to 170 μ l of 85 % MeOH (v/v). Immediately afterwards 20 μl of the internal standard cocktail was added. The internal standard cocktail mixture was prepared by mixing 100 µl of Labeled Amino Acids Standards Set A1 (Cambridge Isotope Laboratories, Inc., Tewksbury, MA), 50 µl of Metabolomics Amino Acids Mix Standard (Cambridge Isotope Laboratories, Inc.), 152 µl of an aqueous solution of 3-methyluric acid-2,4,5,6-13C4,1,3,9-15 N3 (99% atom % 13C, 98 atom % 15 N, 97 % (CP); Sigma-Aldrich, St Louis, MO) at a concentration of 0.5 mg/ml, the internal standard solution was diluted with HPLC water to a final volume of 4.0 ml. The samples were vortexed for 30 s and centrifuged in a benchtop micro centrifuge for 10 min at 17,000g, 4 °C. Supernatant was then transferred to a low absorption polypropylene autosampler vials. Samples were analyzed on a Nexera X2 UHPLC system coupled to an LCMS-8060 triple quadrupole mass spectrometer (Shimadzu Scientific Instruments). 2 μl were injected onto the analytical system and the autosampler was kept at 4 °C during the duration of the batch analysis. Free amino acids were analyzed using the mass spectrometry parameters and chromatographic conditions described in the Shimadzu LC/MS/MS Method Package for Cell Culture Profiling. The method was edited to include stable isotope labeled free amino acids internal standards SRM transitions.

4.4.3. Sulfatides were extracted and purified from serum samples as follows 150 μl of serum was added to 6.0 ml organic extraction solvent (isopropanol:ethyl acetate, 15:85; v:v). Immediately afterward, 20 μl internal standard solution was added (C18:8 mono-sulfo galactosyl(β) ceramide-d3 d18:1-d3/18:0) at a concentration of 10 $\mu g/ml$ (Matreya, State College, PA) and 150 μl of acetic acid. The mixture was vortexed and 4.5 ml of HPLC water was added. Two-phase liquid extraction was performed, the supernatant was transferred to a new tube, and the pellet

was re-extracted. Supernatants were combined and evaporated under nitrogen. Next, 100 µl of 1 M MeOLi in MeOH was added to the dried residues, vortex mixed for 15 s and kept on ice for one hour, vortexed again for 15 s and incubated on ice for another hour. The reaction was then quenched by adding 2.0 mL of aqueous AcOH (0.8 %; v:v). Next, 4.0 ml of Hexane was added, and a 2-phase extraction was performed to eliminate interferences free fatty acids (two cycles). The top organic layer was discarded and the bottom aqueous phase was reextracted (two cycles) with 4.0 ml isopropanol:ethyl acetate (15:85; v:v). Organic extracts were combined and dried under nitrogen. The dried residue was reconstituted in 200 μl of MeOH. 15 μl of reconstituted extract were injected into the analytical system with co-injection of 10 μl of water. The autosampler was kept at 4 °C during the duration of the batch analysis. Sulfatide species profiling was conducted by liquid chromatography-electrospray ionization-tandem mass spectrometry in negative mode, using a Nexera X2 UHPLC coupled to an LCMS-8060 (Shimadzu Scientific Instruments). Lipid separation was achieved by reverse-phase liquid chromatography on a 2.1×50 mm, 1.9 μm Shimadzu C18 HPLC column (Shimadzu Scientific Instruments) using a gradient elution with H₂O/MeCN (1:1; v:v) 0.1 % formic acid and IPA/ MeCN (80:20; v:v) 0.1 % formic acid. This is a semiquantitative method, the relative abundance of sulfatide species are determined based on the peak area ratio with respect to the internal standard. A solution of brain sulfatides at a concentration of 20 µg/ml (Avanti Polar lipids) and sphingosine-1-galactoside-3-sulfate at a concentration of 1 μg/ml (lysosulfatide ammonium salt, Matreya) was used to optimize analytical parameters, and retention time determination.

LabSolutions V 5.114 and LabSolutions Insight V 3.8 SP4 program packages were used for mass spectrometry data processing (Shimadzu Scientific Instruments).

4.5. Proteomics

Mass spectrometry-based proteomic data was deposited to the ProteomeXchange Consortium via the PRIDE partner repository with the dataset identifiers PXD058489 and https://doi.org/10.6019/PXD058489.

4.5.1. Adipose tissue homogenization

Approximately 50 mg of frozen thigh adipose tissue biopsies were homogenized on ice using a Brinkman Homogenizer (Model PT 10/35) in 300 μ l detergent-containing lysis buffer A (50 mM HEPES, pH 7.6, 150 mM NaCl, 20 mM NaPO4, 20 mM beta-glycerophosphate, 10 mM NaF, 2 mM NaVanadate, 2 mM EDTA, 1 % Triton-X100, 10 % glycerol, 2 mM PMSF, 1 mM MgCl₂, 1 mM CaCl₂, 10 μ g/ml leupeptin, 10 μ g/ml aprotinin). Biopsies were homogenized until no visible tissue remained, approximately 3 \times 10 second pulses. Adipose tissue lysates were then incubated on ice for 20 min followed by centrifugation for 20 min at 14,000g, 4 °C. Protein concentration was determined using a Pierce BCA protein assay kit (Thermo Scientific, #23225). The protein concentration averaged approximately 3.5 μ g/ μ l.

4.5.2. In-gel digestion

 $80~\mu g$ of clarified homogenized adipose tissue lysate were separated on a 10~% SDS-PAGE gel and stained with Bio-Safe Coomassie G-250 Stain. Tryptic digestion and desalting were performed as described [72]. In brief, each lane of the SDS-PAGE gel was cut into eight slices, placed in a 0.6 ml LoBind polypropylene tube (Eppendorf), destained twice with 375 μl of 50 % acetonitrile (ACN) in 40 mm NH₄HCO $_3$ and dehydrated with 100 % ACN for 15 min. After removal of the ACN by aspiration, the gel pieces were dried in a vacuum centrifuge for 30 min at 60 °C. Trypsin (250 ng; Sigma-Aldrich) in 20 μl of 40 mM NH₄HCO $_3$ was added and the samples were maintained for 15 min at 4 °C prior to the addition of 50–100 μl of 40 mM NH₄HCO $_3$. The digestion was allowed to proceed at 37 °C overnight and was terminated by addition of 10 μl of 5 % formic acid (FA). After further incubation for 30 min at 37 °C and

centrifugation for 1 min, each supernatant was transferred to a clean LoBind polypropylene tube. The extraction procedure was repeated using 40 μl of 0.5 % FA and the two extracts were combined and dried down to approximately 5–10 μl followed by the addition of 10 μl 0.05 % heptafluorobutyric acid:5 % FA (ν/ν) and incubation at room temperature for 15 min. The resulting peptide mixtures were loaded on a solid phase C18 ZipTip (Millipore, Billerica, MA) and washed with 35 μl 0.005 % heptafluorobutyric acid:5%FA (ν/ν) followed by elution first with 4 μl of 50 % ACN:1 % FA (ν/ν) and then a more stringent elution with 4 μl of 80 % ACN:1 % FA (ν/ν). The eluates were combined and dried completely by vacuum centrifugation and 6 μl of 0.1 % FA (ν/ν) was added followed by sonication for 2 min. 2.5 μl of the final sample was then analyzed by mass spectrometry.

4.5.3. Mass spectrometry and database search

HPLC-ESI-MS/MS was performed in positive ion mode on a Thermo Scientific Orbitrap Fusion Lumos tribrid mass spectrometer fitted with an EASY-Spray Source (Thermo Scientific) as previously described [73]. In brief, NanoLC was performed using a Thermo Scientific UltiMate 3000 RSLCnano System with an EASY Spray C18 LC column (Thermo Scientific, 75 cm \times 75 μ m inner diameter, packed with PepMap RSLC C18 material, 2 µm, #ES805); loading phase for 15 min at 0.300 µl/min; mobile phase, linear gradient of 1-34 % Solvent B in 119 min at 0.220 μl/min, followed by a step to 95 % Buffer B over 4 min at 0.220 μl/min, hold 5 min at 0.250 μ l/min, and then a step to 1 % Buffer B over 5 min at $0.250 \,\mu$ l/min and a final hold for 10 min (total run 159 min); Buffer A = 0.1~% FA/H2O; Buffer B = 0.1~% FA in 80 % ACN. All solvents were liquid chromatography mass spectrometry grade. Spectra were acquired using XCalibur (version 2.3; Thermo Scientific). A "top speed" datadependent MS/MS analysis was performed. Dynamic exclusion was enabled with a repeat count of 1, a repeat duration of 30 s, and an exclusion duration of 60 s. Tandem mass spectra were extracted from Xcalibur 'RAW' files and charge states were assigned using the Proteo-Wizard 3.0 msConvert script using the default parameters. The fragment mass spectra were then searched against the human SwissProt_2018 database (20,413 entries) using Mascot (version 2.6.0; Matrix Science) using the default probability cut-off score. The search variables that were used were: 10 ppm mass tolerance for precursor ion masses and 0.5 Da for product ion masses; digestion with trypsin; a maximum of two missed tryptic cleavages; variable modifications of oxidation of methionine and phosphorylation of serine, threonine, and tyrosine. Crosscorrelation of Mascot search results with X! Tandem was accomplished with Scaffold (version Scaffold 4.8.2; Proteome Software). Probability assessment of peptide assignments and protein identifications were made through the use of Scaffold. Only peptides with ≥95 % probability were considered.

4.5.4. Label-free quantitative proteomics

Progenesis QI for proteomics software (version 2.4; Nonlinear Dynamics Ltd.) was used to perform ion-intensity based label-free quantification as previously described [74]. In brief, in an automated format, raw files were imported and converted into two-dimensional maps (yaxis = time, x-axis = m/z) followed by selection of a reference run for alignment purposes. An aggregate data set containing all peak information from all samples was created from the aligned runs, which was then further narrowed down by selecting only +2, +3, and +4 charged ions for further analysis. The samples were then grouped and a peak list of fragment ion spectra from only the top eight most intense precursors of a feature was exported in Mascot generic file (.mgf) format and searched against the human SwissProt_2018 database (20,413 entries) using Mascot (version 2.4; Matrix Science). The search variables that were used were: 10 ppm mass tolerance for precursor ion masses and 0.5 Da for product ion masses; digestion with trypsin; a maximum of two missed tryptic cleavages; variable modifications of oxidation of methionine and phosphorylation of serine, threonine, and tyrosine; 13C = 1. The resulting Mascot .xml file was then imported into Progenesis,

allowing for peptide/protein assignment, while peptides with a Mascot Ion Score of <25 were not considered for further analysis. Protein quantification was performed using only non-conflicting peptides and precursor ion-abundance values were normalized in a run to those in a reference run (not necessarily the same as the alignment reference run). Principal Component Analysis (PCA) and unbiased hierarchal clustering analysis and accompanying heat map visualization was performed in Perseus [75], while Volcano plots were generated in Python with Matplotlib. Gene Ontology and KEGG pathway analyses were performed with Metascape [21].

4.6. Serum analysis

Leptin (ALPCO, #11-LEPHU-E01) as well as high molecular weight and total adiponectin (ALPCO, #80-ADPHU-E01) were measured with ELISA kits according to the manufacturer's instructions. Human Cytokines and Chemokines (sCD40L, EGF, eotaxin, FGF2, FLT3 ligand, fractalkine, G-CSF, GM-CSF, GRO α , IFN α 2, IFN γ , IL1 α , IL1 β , IL1RA, IL2, IL3, IL4, IL5, IL6, IL7, IL8, IL9, IL10, IL12p40, IL12p70, IL13, IL15, IL17A, IL17E/IL25, IL17F, IL18, IL22, IL27, IP10, MCP1, MCP3, MCSF, MDC (CCL22), MIG, MIP1 α , MIP1 β , PDGF-AA, PDGF-AB/BB, RANTES, TGF α , TNF α , TNF β , VEGFA) were measured by Eve Technologies in their Human Cytokine/Chemokine 48-Plex Discovery Assay (#HD48).

4.7. Abbreviations

Gene (human reference genome (GRCh38)) and protein name abbreviations are following the HUGO gene nomenclature committee recommendations (www.genenames.org)

4.8. Statistical analysis

In general, statistics were perfomed with Python (version 3.12.1). Pearson correlation coefficient and p-value for correlation testing was performed with the function scipy.stats.pearsonr. Two-sampled t-tests (scipy.stats.ttest_ind), one-way ANOVAs (scipy.stats.f_oneway) and two-way ANOVAs (statsmodels.formula.api.ols, anova_lm(model, type = 2)) were used as indicated. Statsmodels (version 0.14.2) was used in Python. sklearn.decomposition.PCA was used for Principal Component Analysis (PCA). False Discovery Rate (FDR) was calculated to correct p-values for multiple comparisons with the Benjamini-Hochberg method (statsmodels.stats.multitest.multipletests method='fdr_bh'). Analysis of covariane (ANCOVA) was performed with statsmodels.api.smf.OLS and formulas $f\{dep_vars_str\} \sim C(Condition) + Age'$, $f\{dep_vars_str\} \sim C(Condition) + BMI + Age'$, or $f\{dep_vars_str\} \sim C(Condition) + BMI + Age'$, or $f\{dep_vars_str\} \sim C(Condition) + BMI + Age'$, or $f\{dep_vars_str\} \sim C(Condition) + BMI + Age'$.

Multivariate analysis of covariance (MANCOVA) was performed with statsmodels.multivariate.manova and formula $f\{dep_vars_str\} \sim C$ (Condition) + BMI + Age + C(Menopause)'. MANCOVA statistical tests Wilks' lambda, Pillai's trace, Hotelling-Lawley trace, Roy's greatest root were performed with statsmodels.multivariate.manova.MANOVA. $mv_test.$

All statistical information regarding Metascape (version 3.5.20240901) can be found online (www.metascape.org/gp/index.htm l#/menu/release_history).

4.9. Machine learning

We implemented multiple supervised learning methods to generate a classification prediction tool with Python (version 3.12.1). The following Python libraries included in scikit learn (or sklearn; stable version 1.4.2) were used: Support Vector Machine (SVM, sklearn.svm. SVC), ElasticNet (Python: sklearn.linear_model.ElasticNet), Random Forest (Python: sklearn.ensemble.RandomForestClassifier). The dataset was first loaded into a pandas DataFrame and split into features and target variables. We then divided the data into training (80 %) and

testing (20 %) sets to evaluate the model's performance (Python: sklearn.model_selection.train_test_split). Feature scaling was applied to standardize the features, ensuring they have a mean of 0 and a standard deviation of 1 (Python: sklearn.preprocessing.StandardScaler or Min-MaxScaler). After training, the models were used to make predictions on the test set. The performance of the model was assessed using metrics such as accuracy, precision, recall, and the F1-score (Python: sklearn. metrics.classification report or confusion matrix). For cross-validation 5-fold CV mean \pm SD was calculated (Python: sklearn.model_selection. cross_val_score). Feature importance was calculated using permutation_importance (Python: sklearn.inspection).

CRediT authorship contribution statement

Leon G. Straub: Writing - review & editing, Writing - original draft, Visualization, Validation, Supervision, Software, Resources, Project administration, Methodology, Investigation, Funding acquisition, Formal analysis, Data curation, Conceptualization. Jan-Bernd Funcke: Writing - review & editing, Writing - original draft, Methodology, Data curation, Conceptualization. Nolwenn Joffin: Writing - review & editing, Writing - original draft, Methodology, Conceptualization. Chanmin Joung: Writing - review & editing, Writing - original draft, Methodology. Sara Al-Ghadban: Writing - review & editing, Writing original draft, Methodology, Formal analysis. Shangang Zhao: Writing - review & editing, Writing - original draft, Formal analysis. Qingzhang **Zhu:** Writing – review & editing, Writing – original draft, Methodology. Ilja L. Kruglikov: Writing - review & editing, Writing - original draft, Formal analysis. Yi Zhu: Writing - review & editing, Writing - original draft, Formal analysis. Paul R. Langlais: Writing - review & editing, Writing – original draft, Methodology, Formal analysis, Data curation. Ruth Gordillo: Writing - review & editing, Writing - original draft, Methodology, Formal analysis, Data curation. Karen L. Herbst: Writing - review & editing, Writing - original draft, Supervision, Funding acquisition, Data curation, Conceptualization. Philipp E. Scherer: Writing - review & editing, Writing - original draft, Visualization, Validation, Supervision, Resources, Project administration, Methodology, Investigation, Funding acquisition, Formal analysis, Data curation, Conceptualization.

Declaration of competing interest

The authors declare that they have no known competing financial interests or personal relationships that could have appeared to influence the work reported in this paper.

Acknowledgements

LGS was supported by the Deutsche Forschungsgemeinschaft (DFG, German Research Foundation) grant #444933586. The Lipedema Foundation funded some of this work (Research Awards Program). This research was supported in part by the computational resources provided by the BioHPC supercomputing facility Department of Bioinformatics, UTSWMC. We thank the UTSW Metabolic Core Unit for the sample analysis and Shimadzu Scientific Instruments for the collaborative efforts in mass spectrometry technology resources.

Appendix A. Supplementary data

Supplementary data to this article can be found online at https://doi. org/10.1016/j.metabol.2025.156191.

References

[1] Herbst KL, Kahn LA, Iker E, Ehrlich C, Wright T, McHutchison L, et al. Standard of care for lipedema in the United States. Phlebology J Venous Dis 2021;36(779-96). https://doi.org/10.1177/02683555211015887.

[2] WOLD EAHJ LE, ALLEN EV. Lipedema of the legs: a syndrome characterized by fat legs and edema. Ann Intern Med 1951;34. https://doi.org/10.7326/0003-4819-34-

- [3] Dinnendahl R, Tschimmel D, Löw V, Cornely M, Hucho T. Non-obese lipedema patients show a distinctly altered quantitative sensory testing profile with high diagnostic potential. PAIN Rep 2024;9. https://doi.org/10.1097/ 000000115
- Kruppa P, Georgiou I, Biermann N, Prantl L, Klein-Weigel P, Ghods M. Lipedema—pathogenesis, diagnosis, and treatment options. Dtsch Arztebl Int 2020. https://doi.org/10.3238/arztebl.2020.0396.
- [5] Forner-Cordero I, Szolnoky G, Forner-Cordero A, Kemeny L. Lipedema: an overview of its clinical manifestations, diagnosis and treatment of the disproportional fatty deposition syndrome - systematic review. Clin Obes 2012;2 (86–95). https://doi.org/10.1111/j.1758-8111.2012.00045.x.
- Eakin GS, Peterson S. Lipedema: A current understanding of its pathology and natural history version 1-May 2023. 2023.
- [7] Peprah K, MacDougall D. Liposuction for the treatment of lipedema: a review of clinical effectiveness and guidelines. Ottawa (ON). 2019.
- Ghods M, Kruppa P. Surgical treatment of lipoedema. Handchir Mikrochir P 2018; 50:400-11. https://doi.org/10.1055/a-0767-6808
- [9] Kruppa P, Georgiou I, Schmidt J, Infanger M, Ghods M. A 10-year retrospective before-and-after study of lipedema surgery: patient-reported lipedema-associated symptom improvement after multistage liposuction. Plast Reconstr Surg 2022;149: 529e-41e. https://doi.org/10.1097/Prs.0000000000008880.
- [10] Herbst KL, Hansen EA, Cobos Salinas LM, Wright TF, Larson EE, Schwartz JS. Survey outcomes of lipedema reduction surgery in the United States. Plast Reconstr Surg Global Open 2021;9. https://doi.org/10.1097/gox.0000000000003
- [11] Duhon BH, Phan TT, Taylor SL, Crescenzi RL, Rutkowski JM. Current mechanistic understandings of lymphedema and lipedema: tales of fluid, fat, and fibrosis. Int J Mol Sci 2022;23. https://doi.org/10.3390/ijms23126621.
- Aday AW, Donahue PMC, Garza M, Crain VN, Patel NJ, Beasley JA, et al. National survey of patient symptoms and therapies among 707 women with a lipedema phenotype in the United States. Vasc Med 2023;29(36-41). https://doi.org/ 10.1177/1358863x231202769.
- [13] Kruglikov IL, Scherer PE. Control of adipose tissue cellularity by the terminal complement cascade. Nat Rev Endocrinol 2023;19(679-80), https://doi.org/ 10.1038/s41574-023-00900-w
- [14] Kruglikov IL, Joffin N, Scherer PE. The MMP14-caveolin axis and its potential relevance for lipoedema, Nat Rev Endocrinol 2020;16(669-74), https://doi.org/ 10.1038/s41574-020-0395-z
- [15] Child AH, Gordon KD, Sharpe P, Brice G, Ostergaard P, Jeffery S, et al. Lipedema: an inherited condition, Am J Med Genet A 2010;152A:970-6, https://doi.org/ 10.1002/aimg.a.33313.
- [16] Herbst KL. Rare adipose disorders (RADs) masquerading as obesity. Acta Pharmacol Sin 2012;33(155-72). https://doi.org/10.1038/aps.2011.153.
- Allen E, Hines E, Hines E. Lipedema of the legs: a syndrome characterized by fat legs and orthostatic edema. Proc Staff Meet Mayo Clin 1940:184-7.
- [18] Koh SJ, Hyun YJ, Choi SY, Chae JS, Kim JY, Park S, et al. Influence of age and visceral fat area on plasma adiponectin concentrations in women with normal glucose tolerance, Clin Chim Acta 2008:389(45-50), https://doi.org/10.1016/j. ca.2007.11.017.
- [19] Scherer PE. The multifaceted roles of adipose tissue—therapeutic targets for diabetes and beyond: the 2015 banting lecture. Diabetes 2016;65(1452-61). https://doi.org/10.2337/db16-0339.
- Abella V, Scotece M, Conde J, Pino J, Gonzalez-Gay MA, Gómez-Reino JJ, et al. Leptin in the interplay of inflammation, metabolism and immune system disorders. Nat Rev Rheumatol 2017;13(100-9). https://doi.org/10.1038/nrrheum.2016.209.
- [21] Zhou Y, Zhou B, Pache L, Chang M, Khodabakhshi AH, Tanaseichuk O, et al. Metascape provides a biologist-oriented resource for the analysis of systems-level datasets. Nat Commun 2019;10. https://doi.org/10.1038/s41467-019-09234-6
- [22] Pan JB, Hu SC, Shi D, Cai MC, Li YB, Zou Q, et al. PaGenBase: a pattern gene database for the global and dynamic understanding of gene function. PloS One 2013;8(e80747). https://doi.org/10.1371/journal.pone.0080747
- Consortium GO. Gene ontology consortium: going forward. Nucleic Acids Res 2014;43:D1049-56. https://doi.org/10.1093/nar/gku1179
- Consortium GO. The gene ontology resource: 20 years and still GOing strong. Nucleic Acids Res 2019;47:D330-8. https://doi.org/10.1093/nar/gky1055
- Kanehisa MKEGG. Kyoto encyclopedia of genes and genomes. Nucleic Acids Res
- 2000;28(27–30). https://doi.org/10.1093/nar/28.1.27.
 [26] Kanehisa M, Furumichi M, Sato Y, Kawashima M, Ishiguro-Watanabe M. KEGG for taxonomy-based analysis of pathways and genomes. Nucleic Acids Res 2023;51: D587-92, https://doi.org/10.1093/nar/gk
- [27] Han H, Shim H, Shin D, Shim JE, Ko Y, Shin J, et al. TRRUST: a reference database of human transcriptional regulatory interactions. Sci Rep 2015;5. https://doi.org/
- [28] Allen M, Schwartz M, Herbst KL. Interstitial fluid in lipedema and control skin. Women's. Health Rep 2020;1(480–7). https://doi.org/10.1089/whr.2020.0086.
- Yang WS, Lee WJ, Funahashi T, Tanaka S, Matsuzawa Y, Chao CL, et al. Plasma adiponectin levels in overweight and obese Asians. Obes Res 2002;10(1104-10). https://doi.org/10.1038/oby.2002.150
- Goropashnaya AV, Herron J, Sexton M, Havel PJ, Stanhope KL, Plaetke R, et al. Relationships between plasma adiponectin and body fat distribution, insulin sensitivity, and plasma lipoproteins in Alaskan Yup'ik Eskimos: the Center for Alaska Native Health Research study. Metabolism 2009;58(22–9). https://doi.org/ 10.1016/j.metabol.2008.09.002.

- [31] Summers SA, Chaurasia B, Holland WL. Metabolic messengers: ceramides. Nat Metab 2019;1(1051–8). https://doi.org/10.1038/s42255-019-0134-8.
- [32] Choi RH, Tatum SM, Symons JD, Summers SA, Holland WL. Ceramides and other sphingolipids as drivers of cardiovascular disease. Nat Rev Cardiol 2021;18 (701–11). https://doi.org/10.1038/s41569-021-00536-1.
- [33] Pedregosa F, Varoquaux G, Gramfort A, Michel V, Thirion B, Grisel O, et al. Scikitlearn: machine learning in python. J Mach Learn Res 2011;12:2825–30.
- [34] Hao JG, Ho TK. Machine learning made easy: a review of Scikit-learn package in python programming language. J Educ Behav Stat 2019;44(348–61). https://doi. org/10.3102/1076998619832248.
- [35] Morgan S, Reid I, Bendon C, Ishaq M, Shayan R, Pope B, et al. A family-based study of inherited genetic risk in lipedema. Lymphat Res Biol 2024;22(106–11). https://doi.org/10.1089/frb.2023.0065.
- [36] Kempa S, Buechler C, Föh B, Felthaus O, Prantl L, Günther UL, et al. Serum metabolomic profiling of patients with lipedema. Int J Mol Sci 2023;24. https://doi.org/10.3390/ijms242417437.
- [37] Park DJ, Park MW, Lee H, Kim Y-J, Kim Y, Park YH. Development of machine learning model for diagnostic disease prediction based on laboratory tests. Sci Rep 2021:11. https://doi.org/10.1038/s41598-021-87171-5.
- [38] Kruppa P, Gohlke S, Łapiński K, Garcia-Carrizo F, Soultoukis GA, Infanger M, et al. Lipedema stage affects adipocyte hypertrophy, subcutaneous adipose tissue inflammation and interstitial fibrosis. Front Immunol 2023;14. https://doi.org/ 10.3389/fimmu.2023.1223264.
- [39] Ishaq M, Bandara N, Morgan S, Nowell C, Mehdi AM, Lyu R, et al. Key signaling networks are dysregulated in patients with the adipose tissue disorder, lipedema. Int J Obes (Lond) 2021;46(502–14). https://doi.org/10.1038/s41366-021-01002-1
- [40] Friedman JM. Leptin and the endocrine control of energy balance. Nat Metab 2019; 1(754–64). https://doi.org/10.1038/s42255-019-0095-y.
- [41] Straub LG, Scherer PE. Metabolic messengers: adiponectin. Nat Metab 2019;1 (334–9). https://doi.org/10.1038/s42255-019-0041-z.
- [42] Castela I, Morais J, Barreiros-Mota I, Silvestre MP, Marques C, Rodrigues C, et al. Decreased adiponectin/leptin ratio relates to insulin resistance in adults with obesity. Am J Physiol Endocrinol Metab 2023;324:E115–9. https://doi.org/ 10.1152/aipendo.00273.2022.
- [43] Nankam PAN, Cornely M, Kloting N, Bluher M. Is subcutaneous adipose tissue expansion in people living with lipedema healthier and reflected by circulating parameters? Front Endocrinol (Lausanne) 2022;13:1000094. https://doi.org/ 10.3389/fendo.2022.1000094.
- [44] Holland WL, Scherer PE. PAQRs: a counteracting force to ceramides? Mol Pharmacol 2009;75(740–3). https://doi.org/10.1124/mol.109.054817.
- [45] Vasiliauskaité-Brooks I, Sounier R, Rochaix P, Bellot G, Fortier M, Hoh F, et al. Structural insights into adiponectin receptors suggest ceramidase activity. Nature 2017;544(120–3). https://doi.org/10.1038/nature21714.
- [46] Zhu Q, Chen S, Funcke J-B, Straub LG, Lin Q, Zhao S, et al. PAQR4 regulates adipocyte function and systemic metabolic health by mediating ceramide levels. Nat Metab 2024;6(1347–66). https://doi.org/10.1038/s42255-024-01078-9.
- [47] Lopez X, Goldfine AB, Holland WL, Gordillo R, Scherer PE. Plasma ceramides are elevated in female children and adolescents with type 2 diabetes. J Pediatr Endocrinol Metab 2013;26. https://doi.org/10.1515/jpem-2012-0407.
- [48] Blachnio-Zabielska AU, Koutsari C, Tchkonia T, Jensen MD. Sphingolipid content of human adipose tissue: relationship to adiponectin and insulin resistance. Obesity 2012;20(2341–7). https://doi.org/10.1038/oby.2012.126.
- [49] Maceyka M, Spiegel S. Sphingolipid metabolites in inflammatory disease. Nature 2014;510(58–67). https://doi.org/10.1038/nature13475.
- [50] Pushkareva M, Obeid LM, Hannun YA. Ceramide: an endogenous regulator of apoptosis and growth suppression. Immunol Today 1995;16(294–7). https://doi. org/10.1016/0167-5699(95)80184-7
- [51] Brinkmann V, Billich A, Baumruker T, Heining P, Schmouder R, Francis G, et al. Fingolimod (FTY720): discovery and development of an oral drug to treat multiple sclerosis. Nat Rev Drug Discov 2010;9(883–97). https://doi.org/10.1038/ nrd3248
- [52] Mobarak E, Håversen L, Manna M, Rutberg M, Levin M, Perkins R, et al. Glucosylceramide modifies the LPS-induced inflammatory response in macrophages and the orientation of the LPS/TLR4 complex in silico. Sci Rep 2018; 8. https://doi.org/10.1038/s41598-018-31926-0.
- [53] Won JS, Singh AK, Singh I. Lactosylceramide: a lipid second messenger in neuroinflammatory disease. J Neurochem 2007;103(Suppl. 1):180–91. https://doi. org/10.1111/j.1471-4159.2007.04822.x.
- [54] Kruglikov IL, Scherer PE. Is the endotoxin–complement cascade the major driver in lipedema? Trends Endocrinol Metab 2024. https://doi.org/10.1016/j. tem.2024.04.004.

- [55] Hotamisligil GS, Budavari A, Murray D, Spiegelman BM. Reduced tyrosine kinase activity of the insulin receptor in obesity-diabetes. Central role of tumor necrosis factor-alpha. J Clin Investig 1994;94(1543–9). https://doi.org/10.1172/ ici117405
- [56] Distler JHW, Györfi AH, Ramanujam M, Whitfield ML, Königshoff M, Lafyatis R. Shared and distinct mechanisms of fibrosis. Nat Rev Rheumatol 2019;15(705–30). https://doi.org/10.1038/s41584-019-0322-7.
- [57] Streubel MK, Baumgartner A, Meier-Vollrath I, Frambach Y, Brandenburger M, Kisch T. Transcriptomics of subcutaneous tissue of lipedema identified differentially expressed genes involved in adipogenesis, inflammation, and pain. Plast Reconstr Surg Global Open 2024;12. https://doi.org/10.1097/ggx/000000000006388
- [58] Cifarelli V, Smith GI, Gonzalez-Nieves S, Samovski D, Palacios HH, Yoshino J, et al. Adipose tissue biology and effect of weight loss in women with lipedema. Diabetes 2024. https://doi.org/10.2337/db24-0890.
- [59] Vasella M, Wolf S, Francis EC, Grieb G, Pfister P, Reid G, et al. Involvement of the macrophage migration inhibitory factor (MIF) in lipedema. Metabolites 2023;13. https://doi.org/10.3390/metabo13101105.
- [60] Wolf S, Rannikko JH, Virtakoivu R, Cinelli P, Felmerer G, Burger A, et al. A distinct M2 macrophage infiltrate and transcriptomic profile decisively influence adipocyte differentiation in lipedema. Front Immunol 2022;13:1004609. https://doi.org/ 10.3389/fimmu.2022.1004609.
- [61] Felmerer G, Stylianaki A, Hägerling R, Wang A, Ströbel P, Hollmén M, et al. Adipose tissue hypertrophy, an aberrant biochemical profile and distinct gene expression in lipedema. J Surg Res 2020;253(294–303). https://doi.org/10.1016/ i.jss.2020.03.055.
- [62] Al-Ghadban S, Cromer W, Allen M, Ussery C, Badowski M, Harris D, et al. Dilated blood and lymphatic microvessels, angiogenesis, increased macrophages, and adipocyte hypertrophy in lipedema thigh skin and fat tissue. J Obes 2019;2019 (1–10). https://doi.org/10.1155/2019/8747461.
- [63] Esmon CT. Interactions between the innate immune and blood coagulation systems. Trends Immunol 2004;25(536–42). https://doi.org/10.1016/j. it 2004 08 003
- [64] Weidmann H, Heikaus L, Long AT, Naudin C, Schlüter H, Renné T. The plasma contact system, a protease cascade at the nexus of inflammation, coagulation and immunity. Biochim Biophys Acta (BBA) Mol Cell Res 2017;1864(2118–27). https://doi.org/10.1016/j.bbamcr.2017.07.009.
- [65] Kruglikov IL, Scherer PE. Is the endotoxin-complement cascade the major driver in lipedema? Trends Endocrinol Metab 2024;35(769–80). https://doi.org/10.1016/j. tem.2024.04.004.
- [66] Kruglikov II., Scherer PE. Pathophysiology of cellulite: possible involvement of selective endotoxemia. Obes Rev 2022;24. https://doi.org/10.1111/obr.13517.
- [67] Câmara NOS, Zampell JC, Yan A, Elhadad S, Avraham T, Weitman E, et al. CD4+ cells regulate fibrosis and lymphangiogenesis in response to lymphatic fluid stasis. PloS One 2012;7. https://doi.org/10.1371/journal.pone.0049940.
- [68] Alim MA, Grujic M, Ackerman PW, Kristiansson P, Eliasson P, Peterson M, et al. Glutamate triggers the expression of functional ionotropic and metabotropic glutamate receptors in mast cells. Cell Mol Immunol 2020;18(2383–92). https://doi.org/10.1038/s41423-020-0421-z.
- [69] Cruzat V, Macedo Rogero M, Noel Keane K, Curi R, Newsholme P. Glutamine: metabolism and immune function, supplementation and clinical translation. Nutrients 2018;10. https://doi.org/10.3390/nu10111564.
- [70] Wernerman J. Clinical use of glutamine supplementation. J Nutr 2008;138: 20405–204045. https://doi.org/10.1093/in/138.10.20405.
- [71] Fürst P, Alteheld B, Stehle P. Why should a single nutrient—glutamine—improve outcome? Clin Nutr Suppl 2004;1(3–15). https://doi.org/10.1016/j. clnu.2004.07.006.
- [72] Kruse R, Krantz J, Barker N, Coletta RL, Rafikov R, Luo M, et al. Characterization of the CLASP2 protein interaction network identifies SOGA1 as a microtubuleassociated protein. Mol Cell Proteomics 2017;16(1718–35). https://doi.org/ 10.1074/mcp.RA117.000011.
- [73] Parker SS, Krantz J, Kwak EA, Barker NK, Deer CG, Lee NY, et al. Insulin induces microtubule stabilization and regulates the microtubule plus-end tracking protein network in adipocytes. Mol Cell Proteomics 2019;18(1363–81). https://doi.org/ 10.1074/mcn.RA119.001450.
- [74] Uhlorn JA, Husband NA, Romero-Aleshire MJ, Moffett C, Lindsey ML, Langlais PR, et al. CD4(+) T cell-specific proteomic pathways identified in progression of hypertension across postmenopausal transition. J Am Heart Assoc 2021;10 (e018038). https://doi.org/10.1161/JAHA.120.018038.
- [75] Tyanova S, Cox J. Perseus: a bioinformatics platform for integrative analysis of proteomics data in cancer research. Methods Mol Biol 2018;1711(133–48). https://doi.org/10.1007/978-1-4939-7493-1_7.